MASTER THESIS

Creating weight bearing 3D models of the lower limbs

Koen Verdonschot, BSc.

Technical Medicine
Faculty of Science & Technology (TNW)
University of Twente

EXAMINATION COMMITTEE
Prof.dr.ir. C.H. Slump
Dr. R.J.H. Custers
Drs. P.A. van Katwijk
Dr.ir. R. Fluit
Dr. N. van Egmond
H.C. Nguyen, MSc

UMC Utrecht UNIVERSITY OF TWENTE.

Master Thesis

Technical Medicine

Medical Imaging and Interventions

CREATING WEIGHT BEARING 3D MODELS OF THE LOWER LIMBS

Koen Hubertus Maria Verdonschot, BSc.

A thesis submitted for the degree of

Master of Science in Technical Medicine

GRADUATION COMMITTEE

CHAIRMAN & TECHNICAL SUPERVISOR	Prof. Dr. Ir. C.H. Slump Faculty of Electrical Engineering, Mathematics & Computer Science (EEMCS), Robotics and Mechatronics (RAM) University of Twente, Enschede, The Netherlands
MEDICAL SUPERVISOR	Dr. R.J.H. Custers Department of Orthopaedic Surgery, UMC Utrecht UMC Utrecht, Utrecht, The Netherlands
PROCESS SUPERVISOR	Drs. P.A. van Katwijk Faculty of Science and Technology (TNW) Technical Medicine University of Twente, Enschede, The Netherlands
EXTERNAL COMMITTEE MEMBER	Dr. Ir. R. Fluit Faculty of Engineering Technology (ET), Biomechanical Engineering (BE) University of Twente, Enschede, The Netherlands
ADDITIONAL COMMITTEE MEMBERS	Dr. N. van Egmond Department of Orthopaedic Surgery, UMC Utrecht UMC Utrecht, Utrecht, The Netherlands
	H.C. Nguyen, MSc Department of Orthopaedic Surgery, UMC Utrecht UMC Utrecht, Utrecht, The Netherlands

ABSTRACT

Purpose: Lower limb malalignment is an important factor for young and active patients presenting knee osteoarthritis. Realignment osteotomy has proven to be highly effective as surgical treatment for those patients. An accurate preoperative plan is important for a successful outcome. The gold standard for preoperative osteotomy planning of the lower limbs requires weight-bearing whole leg radiographs (WLR). However, sagittal and transversal deformities can be overlooked on these 2D images. Additional 3D CT scans can provide this information but lack the weight-bearing aspect. The combination of 3D information with weight-bearing is especially useful in the care of patients presenting knee osteoarthritis with deformities in multiple planes. The aim of this research is to investigate the possibility of creating weight bearing 3D models of the lower limbs from a CT scan and a single WLR of the patient.

Materials & Methods: Software was developed for manually aligning 3D models onto a single anteroposterior weight bearing WLR. This study included 30 patients with available CT scans. Digitally reconstructed (whole leg) radiographs (DRR) and anatomical 3D models were computed from these CT scans. Three raters performed manual registrations of the anatomical 3D models onto the DRRs using the software. A second method was developed for automation of the 3D-2D registration using an optimization algorithm. Anatomical 3D models of ten patients were registered using the semi-automatic algorithm with three different optimization algorithms. The registered 3D models were compared to the 3D models in original state. Errors were expressed in absolute distances and errors measured in the lower limb geometry: frontal hip-knee-ankle angle (HKA), sagittal HKA, joint line convergence angle (JLCA), and tibiofemoral rotation.

Results: Mean registration error of the manual registration was highest in sagittal plane (6.10mm ± 4.47mm) compared to the anteroposterior plane (0.89mm ± 0.39mm). The angular error was highest for the sagittal HKA and tibiofemoral rotation, respectively 1.63° (± 1.28°) and 1.69° (± 1.33°), and lowest for frontal HKA and the joint line conversion angle, respectively 0.60° (± 0.60°) and 0.54° (± 0.64°).

Mean registration error in the XYZ dimension was 30.10mm for the Genetic Algorithm (GA), 12.83mm for the multi objective GA, and 33.81mm for the surrogate algorithm. The angular errors were highest for the genetical algorithm (GA), with error of the frontal HKA being 2.32° (± 2.59°) and 1.57° (±1.18°) for the JLCA, while they were lowest when using a multi objective GA, 1.04° (±1.10°) for the frontal HKA and 0.93° (±0.77°) for the JLCA. Variation in results is high though.

Conclusion: Manual registration of 3D models onto 2D DRRs provide accurate results in the antero-posterior plane, but results are less accurate in the sagittal plane. Semi-automatic registration using optimization algorithms is in the current form not accurate enough for clinical use.

LIST OF ABBREVIATIONS

2D	Two Dimensional
3D	Three Dimensional
ACI	Autologous Chondrocyte Implants
AI	Artificial Intelligence
AP	Anteroposterior
CORA	Center Of Rotation Angulation
CT	Computer Tomography
DFC	Distal Femoral Condyles
DFO	Distal Femoral Osteotomy
DRR	Digitally Reconstructed Radiograph
FMA	Femoral Mechanical Axis
HKA	Hip Knee Ankle Angle
HTO	High Tibial Osteotomy
ICC	Intraclass Correlation Coefficient
ICP	Iterative Closest Point
JLCA	Joint Line Conversion Angle
LDTA	Lateral Distal Tibia Angle
LPFA	Lateral Proximal Femur Angle
LUT	LookUp Table
MAD	Mean Average Distance
MFC	Microfracturing
mLDFA	Mechanical Lateral Distal Femur Angle
mMPTA	Mechanical Medial Proximal Tibia Angle
OA	Osteo Arthritis
OATS	Osteochondral Autograft Transfer System
PACS	Picture Archiving and Communications System
PFC	Posterior Femoral Condyles
PTP	Posterior Tibia Plateau
TKA	Total Knee Arthroplasty
TMA	Tibial Mechanical Axis
UKA	Unicompartmental Knee Arthroplasty
UMC	University Medical Centre
WLR	Weight Bearing Longleg Radiograph

TABLE OF CONTENTS

INTRODUCTION

Unicompartmental Osteoarthritis

The knee is a complex joint consisting of three articulating surfaces, multiple strong ligaments and muscles for stability and load distribution (1). Normal load distribution in the knee is not equally distributed between the lateral and the medial knee compartment. In standing position, approximately 66% of the load is accounted for by the medial compartment (2,3). Malalignment of the knee can further increase the load imbalance. This load imbalance, most commonly caused by varus or valgus of the knee, can cause early unicompartmental osteoarthritis (OA) (4–6).

Unicompartmental OA is a major clinical challenge, especially in patients under 50 years of age with an active lifestyle. They may experience pain, instability, and limited range of motion. These symptoms can limit the ability of the patient to perform his or her work, sport activities and even daily activities. Early detection of OA with adequate early conservative intervention can slow disease progression and reduce complaints. Conservative treatment is useful for mild to moderate knee OA. The Kellgren and Lawrence classification is a common classification system for grading of AO (7,8). Figure 1 shows the classification grades and description of the grades applied to the knee. Grade 3 indicates moderate OA. Possible conservative treatments are physical therapy, brace treatment, pain medication, intra-articular injections wit corticosteroids or hyaluronic acid, and life style adjustments such as losing weight (9). These treatments are not able to heal damaged cartilage, but focusses on extending the time to surgical intervention by relieving pain and improving function (9–11).

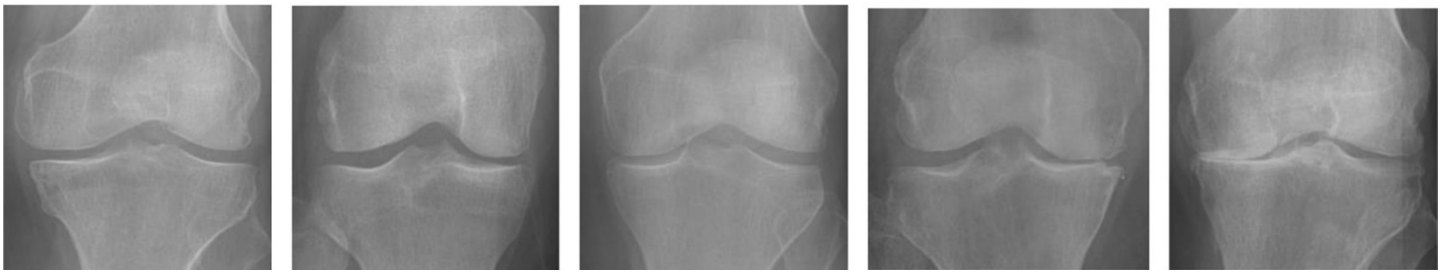

Grade 0	Grade 1	Grade 2	Grade 3	Grade 4
None	**Doubtful**	**Minimal**	**Moderate**	**Severe**
No features of osteoarthrosis	Doutful joint space narrowing and possible osteophytic lipping	Definite osteophytes and minimal joint space narrowing	Moderate multiple osteophytes and moderate joint space narrowing	Large osteophytes, marked narrowing of joint space, subchondral sclerosis

FIGURE 1: THE KELLGREN AND LAWRENCE CLASSIFICATION SYSTEM FOR OSTEOARTHRITIS APPLIED TO THE KNEE. (ILLUSTRATION ADAPTED FROM *CHEN ET AL. FULLY AUTOMATIC KNEE OSTEOARTHRITIS SEVERITY GRADING USING DEEP NEURAL NETWORKS WITH A NOVEL ORDINAL LOSS* (12))

Surgical intervention is indicated when non-surgical treatments fail to offer pain relief or increased function in cases of unicompartmental OA. Possible interventions are unicompartmental knee arthroplasty (UKA) and realignment surgery. UKA and realignment surgery have differing and partial overlapping indications, therefore good patient selection is crucial for both treatments. Patients' age, presence of deformities in the lower limb and severity of the OA are important selection criteria. UKA has a limited lifespan and enables a limited range of motion and activity level after surgery, compared to an osteotomy (13,14). UKA focusses on pain reduction and re-enabling a mostly sedentary lifestyle for patients and is therefore less suitable for young (<60 years of age) and active patients who aim to remain active. The main differentiating criterion for either UKA or realignment surgery is the presence of a deformity in the femur or tibia. If severe unicompartmental OA is present but no deformity in the bone, UKA is indicated (13,15). Both methods have shown good survival rates at 10 years (16,17).

In summary, UKA is more suited for elder patients (>60 years of age) with low to moderate activity levels, no lower limb deformities and low degree of malalignment (up to 5° of varus or valgus) in the lower limbs. On the other hand, realignment surgery is better suited for younger patients (<60 years of age) with a high activity level and lower limb deformities. In a small group of patients between 55 to 65 years old, both an HTO or UKA can be considered (13). In the group of younger patients, a knee osteotomy is therefore most favourable due to longer survival times and better outcomes. Additionally, an osteotomy can be used in the treatment of localized cartilage defects. Combining cartilage resurfacing procedures with realignment surgery produces better outcomes. Several articles have found the combination of an osteotomy with cartilage repair for isolated cartilage damage improves outcomes for the patients (18–20). These cartilage repairs can be microfracturing (MFC), autologous chondrocyte implants (ACI), or osteochondral autograft transfer system (OATS) (21).

Osteotomies around the knee

The primary aim of an osteotomy is to shift the load-bearing axis from the OA compartment to the contralateral healthy compartment. This reduces the load on the arthritic side of the knee to reduce pain and improve clinical outcomes.

Osteotomies around the knee can be subdivided according to the used surgical technique:

1. The location of the osteotomy; proximal tibia or distal femur
2. The side of the osteotomy; on the medial or the lateral side
3. The osteotomy technique; open wedge or closed wedge

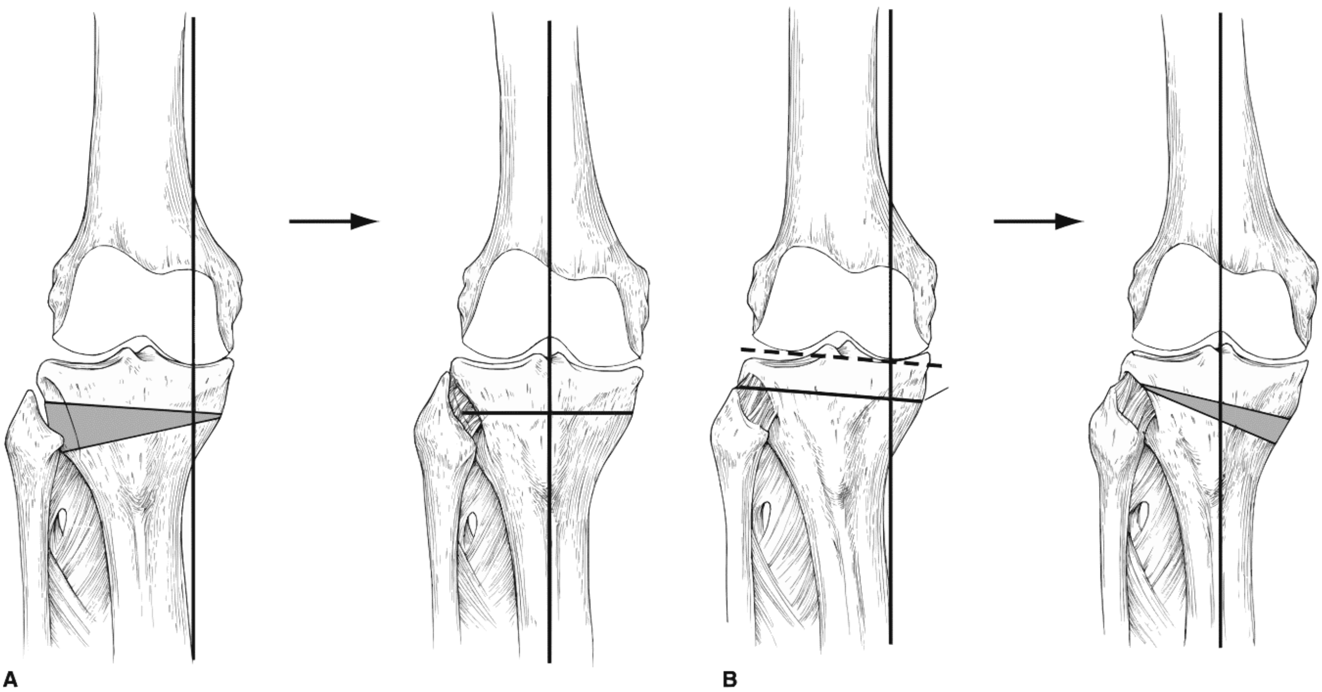

FIGURE 2: ILLUSTRATION OF THE CLOSING WEDGE TECHNIQUE (A) AND THE OPENING WEDGE TECHNIQUE (B) IN A HIGH TIBIAL OSTEOTOMY. THE BLACK VERTICAL LINE INDICATES THE MECHANICAL AXIS OF THE LEG AND SHIFTS TO THE HEALTHY COMPARTMENT AFTER THE OSTEOTOMY. (ILLUSTRATION ADAPTED FROM *B. ASHEESH ET AL., MANAGEMENT OF THE POSTTRAUMATIC ARTHRITIC KNEE* (22))

During a closed wedge osteotomy a wedge is extracted from the bone, where after the gap is closed and fixated. In an open wedge osteotomy, the osteotomy is wedged open and fixated using an angular stable plate. Figure 2 illustrates both techniques for treatment of a varus deformity in the proximal tibia.

With the introduction of the first modern osteotomies in the 1960s, a closing wedge osteotomy (CWO) in the tibia fixated with staples was the preferred technique. It was thought that this type of osteotomy was more stable, permitted a shorter time to recovery and faster load bearing capabilities for the patient. With the introduction of the total knee arthroplasty (TKA) the use of osteotomies around the knee decreased significantly. Improvements in surgical techniques, fixation materials, and postoperative rehabilitation led to significantly better outcomes for osteotomies around the knee, compared to earlier techniques (23). This made the osteotomy a viable option again. Additional improvements in material and design of the fixation plates and the evolution to angular stable plates has allowed the patients with an open wedge osteotomy for partial weight bearing post-surgery. This resulted in improved patient outcomes 6 months and 1 year postoperative (24). Additional advantage of a medial open wedge high tibial osteotomy over the closed wedge lateral technique is the absence of additional fibular osteotomies. Fibular osteotomies can induce peroneal nerve damage. Lastly, open wedge osteotomies tend to be more accurate due to an increased control over the correction perioperatively (25).

Patient selection is important for osteotomies to ensure a good success of the procedure. The international society of arthroscopy, knee surgery and orthopaedic sports medicine (ISAKOS) composed inclusion and exclusion criteria for high tibial osteotomies, which are also applicable to other types of osteotomies (26).

TABLE 1: IN- AND EXCLUSION CRITERIA FOR HIGH TIBIAL OSTEOTOMY (HTO), AS DEFINED BY ISAKOS

Ideal candidate	Possible candidate	No candidate
Isolated medial joint line pain	Flexion contracture < 25°	Flexion contracture > 25°
Age 40-60 years	Age 60-70	Bicompartmental disease
BMI < 30	Moderate, symptomatic PF OA	Previous meniscectomy in compartment to be loaded by HTO
Non smoker	Instability of ACL/PCL/PLC	Prior knee infection
High demand activity (no running or jumping)	Want to participate in all sports	Rheumatoid arthritis
Malalignment < 15°		Obesity
Full range of motion		Possible non compliance
Normal lateral and patellofemoral components		Smoker
OA classification IKDC (A) B, C, D		Soft atrophic appearing on x-ray
Normal ligament balance		Severe femoral bone loss
No notch osteophytes		
Metaphyseal varus, i.e. TBVA > 5°		

The ideal osteotomy candidate is young, healthy, has an active lifestyle, OA limited to one compartment and a malalignment of the knee. The procedure is not recommended for older patients, obese patients, patients with knee co-morbidities, and smokers

Osteotomy planning

Pre-operative planning of osteotomies are a key factor for a successful treatment outcome (27). A pre-operative planning composes an optimal treatment strategy, which determines the correction site, amount of correction and surgical technique. A planning also ensures a more accurate procedure and sufficient correction (28). Pre-operative planning utilizes anteroposterior (AP) 2D whole leg radiographs (WLR) (27). In 2002 extensive guidelines were published by Paley for diagnosing the deformity and composing optimal preoperative planning (29). The most important angles are listed in Table 2 and illustrated in Figure 3. Of most importance is the Mikulicz line; the mechanical axis from the centre of the femoral head to the centre of the ankle joint in the frontal plane. This axis should run slightly medially through the knee, resulting in a slight varus of the knee (27). The measured lower limb geometry forms the basis of the preoperative correction planning. The principle is to correct the deformity at the centre of rotation angulation (CORA). In case of medial knee OA with a varus malalignment, the aim is to overcorrect the stance into slight valgus.

TABLE 2: THE ANGLES AND THEIR NORMAL VALUES DEFINED BY THE MECHANICAL AXES IN THE LOWER LIMB, AS ABLE TO DETERMINE ON AN AP WEIGHT BEARING LONG LEG RADIOGRAPH.

Name	Abbreviation	Normal value
Lateral Proximal Femur Angle	LPFA	90° (85-95°)
Mechanical Lateral Distal Femur Angle	mLDFA	88° (85-90°)
Mechanical Medial Proximal Tibia Angle	mMPTA	87° (85-90°)
Lateral Distal Tibia Angle	LDTA	89° (86-92°)
Joint Line Conversion Angle	JLCA	0°-2°

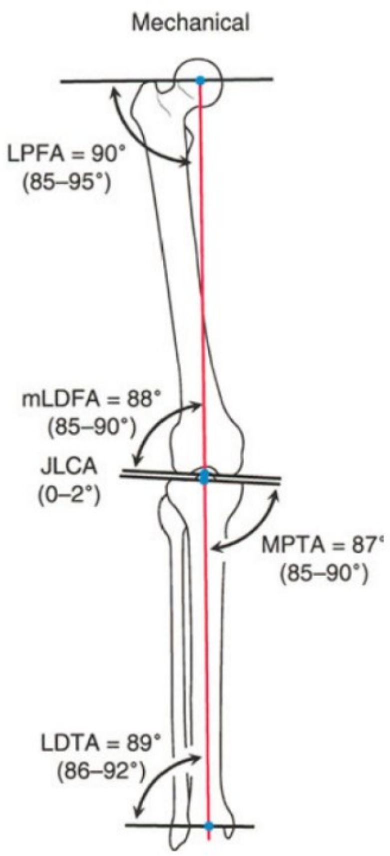

FIGURE 3: A DIAGRAM OF THE LOWER LIMB (FEMUR, TIBIA AND FIBULA) WITH THE MECHANICAL AXES AND THE NORMAL VALUES FOR THE ANGLES. (ILLUSTRATION FROM *D. PALEY, PRINCIPLES OF DEFORMITY CORRECTION* (29))

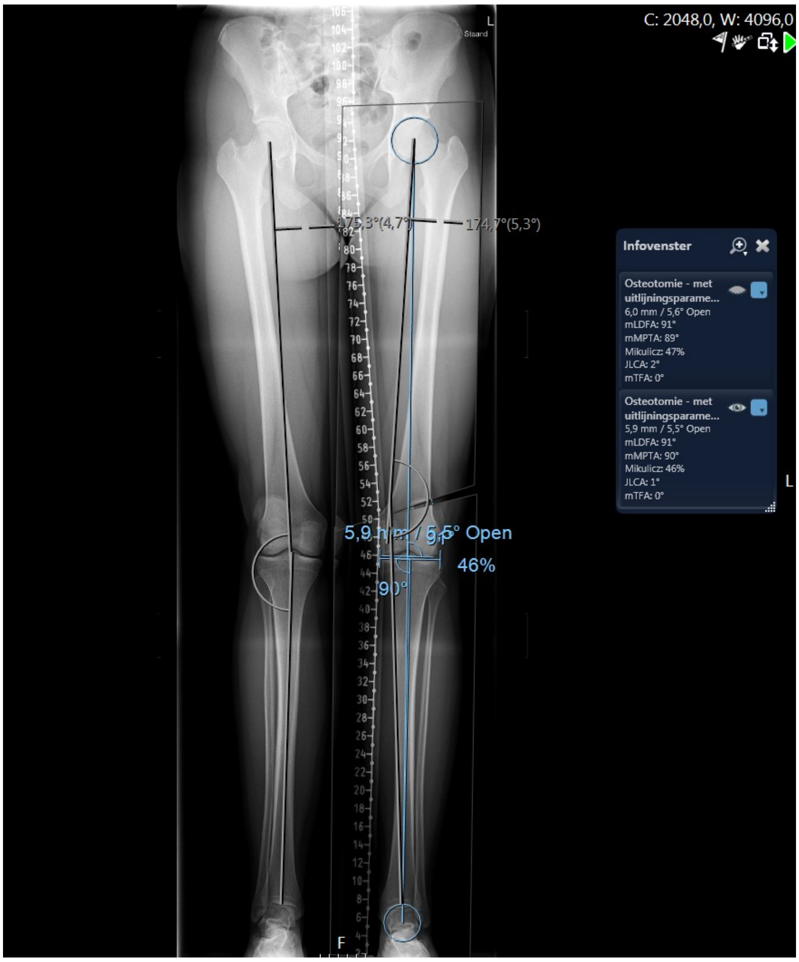

FIGURE 4: SPECIALIZED SOFTWARE, OFTEN EMBEDDED IN THE PACS ENVIRONMENT AIDS THE SURGEON BY AUTOMATICALLY CALCULATING THE VARIOUS ANGLE DURING THE PRE-OPERATIVE OSTEOTOMY PLANNING.

The ideal hip-knee-ankle angel (HKA) after varus correction is between 3-5° of valgus (30). According to Fujisawa the Mikulicz line should run approximately at 63% of width of the tibia plateau for optimal results (31), but recent guidelines call for an individualized overcorrection between 0-6° (32). This reduces the forces on the osteoarthritic compartment and shifts the load towards the non-arthritic side.

Special software tools, embedded in the Picture Archiving and Communication System (PACS) environment, aids the surgeon by automatically calculating the angles while simulating the osteotomy, Figure 4.

3D measurements

Current guidelines for pre-operative osteotomy planning are developed for use with AP standing long leg radiographs. Therefore, sagittal and transversal deformities are not visible and could be overlooked. The current reference for transversal lower limb geometry measurements utilizes Computed Tomography (CT) scans. However, CT scans are obtained with the patient in a non-weight bearing supine position. Weight-bearing is essential for accurate measurements due to soft tissue compression, as non-weight bearing can significantly change the geometry of the lower limb, such as the HKA and the JLCA (33). Additionally, the varus or valgus is often underestimated in non-weight bearing imaging (34). Weight-bearing CT scans have been developed for use with the ankle, but are not usable for the whole lower limb (35). Weight bearing provides added value for the preoperative planning and give information not available on conventional non-weight bearing CT scans

CT scans can be segmented to create 3D models of the bones in the scan. During pre-operative planning 3D models can increase measurement accuracy. The preoperative plan can be translated with 3D models in personalized surgical instruments (PSI). In recent years PSI have become more accessible increasing surgical accuracy with better outcomes for the patients, also in knee realignment (36,37).

Use of 3D models in lower limb realignment surgery has been reported in a few articles, however, none addressed the limitation of the non-weight bearing CT scans. A solution for the lack of 3D information in 2D radiographs and the absence of weight-bearing in 3D CT scans, could be combining the two image modalities with special computer vision software.

3D-2D registration

3D-2D registration is the process of aligning a 3D object with a 2D image. On 2D WLRs depth information is absent, making the 3D-2D registration challenging due to the mismatch in information between the two imaging modalities. Several methods of 3D-2D registration have been investigated in the past. In 2012, a review published by Markelj et al. outlined several of the different methods for 3D-2D registration (38). According to them 3D-2D registration could be performed with intrinsical information from the images or with extrinsic aid of markers fixated on the object. The markers are then used to align the 3D object to the 2D image. However, in the clinical setting markers on the skin can move, making the extrinsic method non-viable. 3D-2D registration is therefore more viable when using the intrinsic data from the images. Markelj et al. divided the intrinsical registration into three methods: feature-based registration, intensity-based registration, and gradient based registration.

The type of data is important for selecting the correct intrinsic 3D-2D registration method. In the University Medical Centre (UMC) Utrecht standardized 2D WLRs are indicated when patients visit the outpatient clinic with unicompartmental OA and/or localized cartilage damage (27). When there is suspicion of rotational and/or sagittal deformities during physical or radiological exam, an additional CT scan is obtained for 3D anatomical models. This workflow results in 2D WLRs with accompanying 3D CT scans (and 3D models) of a patient.

According to Markelj et al., the two main options for 3D-2D registration with the available data are:

1. minimization of the distance between 2D silhouette and contour of projected 3D model
2. optimization of the similarity between 2D image and 2D simulated x-ray from the CT scan

The first method uses the contour of the 3D model and the silhouette of the bone in the WLR to determine the position of the 3D model in the space. When the 3D model is in the same position as in the WLR, the difference between silhouette and contour will be minimal.

The second 3D-2D registration method uses simulated radiographs out of the CT scan, called Digital Reconstructed Radiographs (DRR). By creating DRRs with the CT scan in different positions and orientations and comparing them to the WLR, the position of the CT scan with the highest resemblance to the WLR most is searched.

Figure 5 shows the methods as described by Markelj et al. Method *a* and *d* are two of the possible methods with the data available.

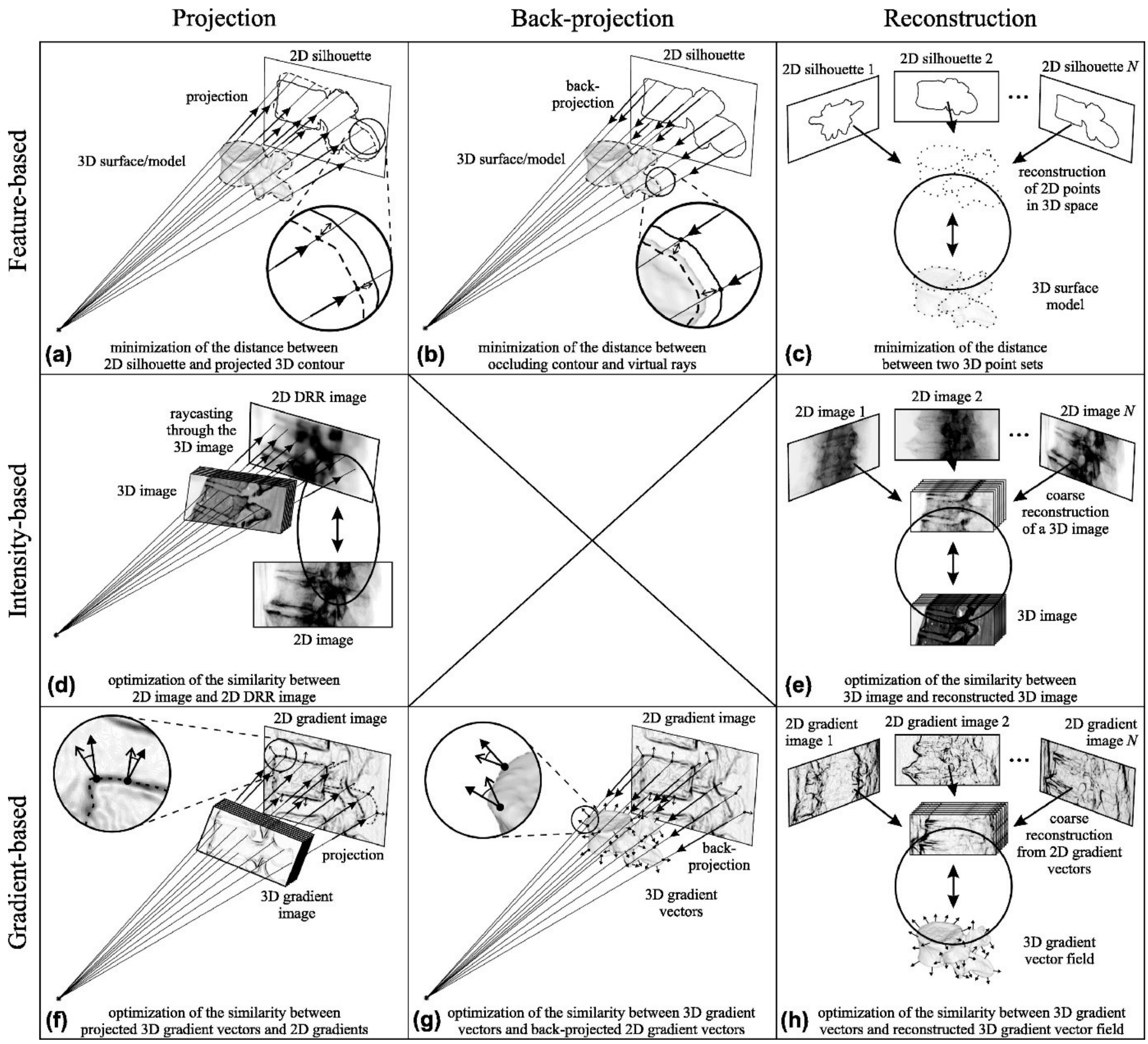

FIGURE 5: THE MAIN METHODS AND DIFFERENTIATORS FOR 3D-2D REGISTRATION AS DEFINED BY MARKELJ ET AL. (*ILLUSTRATION FROM MARKELJ ET AL., A REVIEW OF 3D/2D REGISTRATION METHODS FOR IMAGE-GUIDED INTERVENTIONS* (38))

RESEARCH OBJECTIVES

The problem of 3D-2D for registration of femur and tibia using a single AP WLR has not been solved before. In this study we try to solve this problem and to create weight-bearing 3D models of the lower limb. The problem is researched using both a manual and a semi-automatic approach.

Manual registration has not been widely researched before and isn’t in use for clinical practices at the moment. Independent of this research, software has been made to mimic the projection of the WLR using anatomical 3D models. This software will be used for registering the 3D models to the 2D WLR. The objective is to research the usability of manual software in 3D-2D registration of femur and tibia. Important measures for these are the registration accuracy, measured angles and the time needed to register the models.

Next to researching the viability of manual 3D-2D registration, the step to automation of the process will be made. We hypothesized that automation of the 3D-2D registration could result in a higher accuracy of the registration in less time. The accuracy of the registration is of most importance, but the time needed for registration and the ease of use are also of great importance and will define if a semi-automatic solution is preferable over the manual registration.

For both the manual and the automatic methods, registration accuracy was expressed in the accuracy from model to model, but also if the measurements for knee alignment changed between model pair.

We hypothesize that for both methods the main errors will be present in the sagittal plane, since this information is missing in the 2D WLRs. We also hypothesize that a semi-automatic registration would produce results similar in accuracy, compared to the manual registration, but would be faster in computing the results.

METHOD
MANUAL REGISTRATION

Materials
Registration software
According to the review by Markelj et al. the main options for performing 3D-2D registration using 2D WLRs and 3D CT scans are 1: minimizing the difference of the contour from a projected 3D model of a bone to the contour of the bone in the WLR, or 2: finding the digitally reconstructed radiograph (DRR) of the CT scan which has the closed resemblance to the WLR (38). The second method is much more computationally intensive and more difficult to implement. Therefore, the first method of 3D-2D registration was implemented in software for manual registration. By applying the same projection to the 3D model, as was used in the WLRs, the position can be found where the shadow of the projected 3D models is the same as the object in the WLR. This projection is calculated by formula 1 and illustrated in figure 6:

$$B_x = A_x \frac{B_z}{A_z} \qquad \text{Formula 1}$$

where:

Bx = the screen coordinate
Ax = the model coordinate
Bz = the distance from source to detector
Az = the distance from source to object

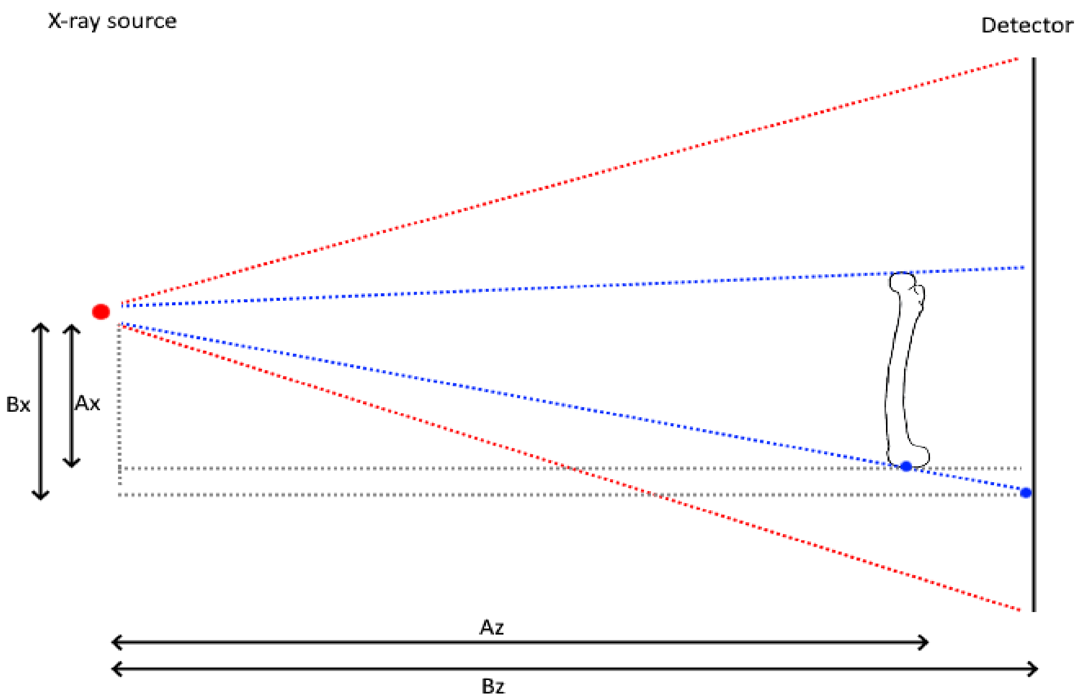

FIGURE 6: THE DIAGRAM ILLUSTRATES THE PERSPECTIVE PROJECTION. THE X-RAY SOURCE IS IMAGINED AS A PERFECT POINT SOURCE. THE TWO BLUE POINTS INDICATE THE TRUE POSITION AND THE PROJECTED POSITION ON THE DETECTOR PLANE.

If the 3D model is in the registered position, the casted shadow of the 3D model will match the bone in the WLR. By adjusting the position and rotation, the projection shadow can be adjusted until the shadow aligns with the WLR. This indicates that the bone model is in the same position as the bone was when making the WLR

Software that implements this method has been developed within the Orthopaedic research group in UMC Utrecht. This software mimics the projection and draws the contour of the projected femur while simultaneously displaying the radiograph, as shown in Figure 7.

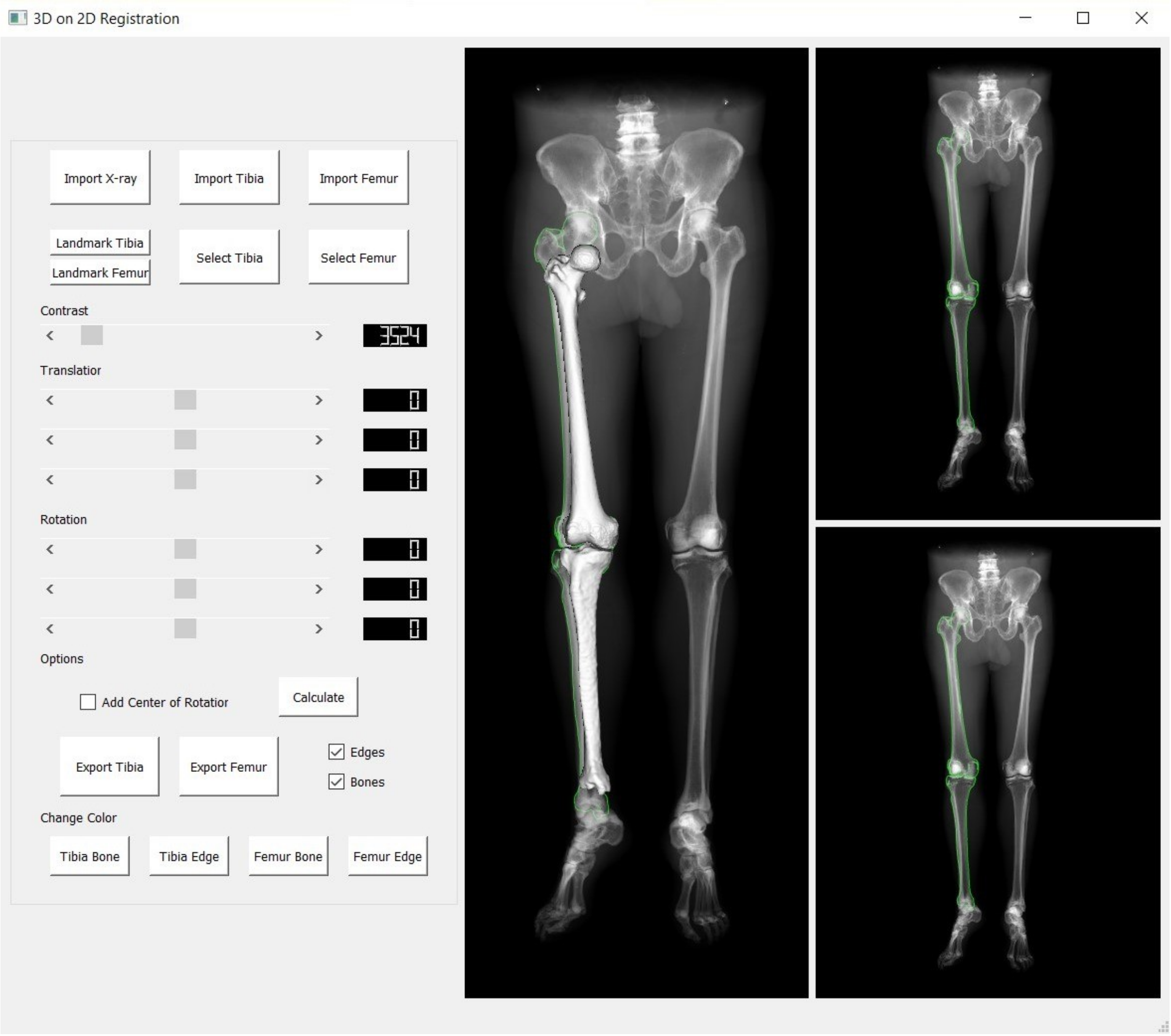

FIGURE 7: THE SOFTWARE DEVELOPED FOR 3D-2D REGISTRATION. BY IMPORTING A WLR AND 3D MODEL, AND ADJUSTING THE POSITION AND ORIENTATION FOR THE 3D MODELS, THE REGISTERED POSITION CAN BE FOUND WHEN THE CONTOUR OF THE PROJECTED 3D MODEL ALIGNS WITH THE BONE IN THE WLR. THE TWO RIGHTMOST WINDOWS CAN BE ZOOMED IN ON SPECIFIC PARTS TO AID WITH FINE ADJUSTMENTS.

Radiographs and 3D models

To test the feasibility of manual 3D-2D registration of the lower limbs using this software, a dataset consisting of WLRs and CT scans with femur and tibia are required. The position of femur and tibia in the WLR has to be known. This is necessary to validate the registration results against the ground truth. The ground truth in this case being the 3D models of femur and tibia segmented from the CT scans. Since no such database exists and since it is very difficult to create such a database from real WLRs and CT scans, the decision was made to construct an artificial database from CT scans.

Using the dataset from the APPROACH study, available in the UMC Utrecht, a dataset consisting of artificial WLRs and 3D models was constructed. The APPROACH database consists of over 60 CT scans and segmented bone structures of the lower limbs. By using the same CT scan to construct the artificial WLR (further called the DRR) and create the 3D models, we know that both the CT scan and the segmented 3D model will give the same projection, when the same projection parameters are applied.

The DRRs were made with MevisLab (Mevislab 3.4.1, Mevis Medical Solutions AG, Bremen, Germany), using the same projection parameters as for conventional WLRs. The distance from X-ray source to detector was set to 2650mm, with the CT-volume placed against the detector in AP direction. The CT-bed, present in the CT scan, is segmented and removed from the scan. Pixel size in the DRR is 0.5mm by 0.5mm. More specific details on creation of the DRRs is provided in the Appendix.

Femur and tibia were segmented from the CT scans with Materialise Mimics (Mimics 23.0, Materialise NV., Leuven, Belgium) to create anatomical 3D models.

From the dataset, the first 30 CT scans were included for the research. In total this provides:

- 30 Digital reconstructed radiographs
- 30 3D models of femur and tibia, right side
- 30 3D models of femur and tibia, left side

Design

The 3D models were randomly rotated and translated from their original reference position and orientation. With the 3D-2D registration software, the 3D models were registered to the DRRs. By manipulating the rotation around the X-, Y- and Z-axis and the position in the X-, Y- and Z-space the projection changes. When the contour of the projected model matches the silhouette of the corresponding bone in the DRR, the 3D model will be in the original position.

This process of registering the 3D model to the DDR was repeated for all 30 DRRs by three raters. By using three raters the variability of the registration accuracy between multiple raters could be tested. Additionally, the first rater performed the registration for all 30 DRRs twice, with two weeks between each registration, to assess repeatability of the registration.

Measurements

The registration process resulted in 60 pairs of femora and tibiae per rater for analysis. Analysis of the registration was performed in two ways:

1. Distance measurements between the reference models and the registered models.
2. The angular and rotational deviations between reference models and registered models.

Distances

A 3D computer model, also called a polygon mesh, is built out of vertices and faces, Figure 8. The vertices have a location in the X-, Y-, and Z-space. From these vertices, edges and faces can be constructed that will form the 3D model. The order of vertices, edges and faces in the model does not change after registration. Locations of each vertex could therefore be directly compared between the reference and the registered model. Euclidean distances were calculated between each vertex pair in the XYZ-dimension, the XY-dimension and the Z-dimension. The XYZ-distance indicated the full distance between each vertex pair. The XY-distances indicated the differences between each vertex pair in the frontal plane. The Z-distances indicated the registration errors made in the sagittal plane. Additionally, Sørensen-Dice coefficients (SDC) were calculated using 2D masks of the reference and

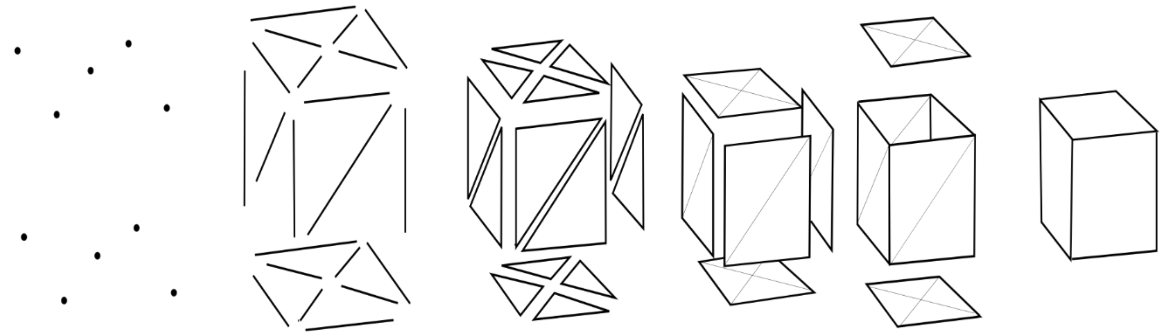

FIGURE 8: 3D MODELS ARE DIVIDED IN SEVERAL SUBSTRUCTURES. THE CONNECTIONS BETWEEN THESE SUBSTRUCTURES FORMS THE POLYGON MESH, THE 3D MODEL. (*ILLUSTRATION FROM WIKIPEDIA, POLYGON MESH* (39))

the registered models. The SDC gives an indication of accuracy of the registration but cannot replace distance measurements. The formula for calculation of the SDC is as follows:

$$SDC = \frac{2|X \cap Y|}{|X|+|Y|} \qquad \text{Formula 2}$$

where:

SDC = the Sørensen-Dice coefficient
X = the 2D surface area of the reference model
Y = the 2D surface area of the registered model

Figure 9 gives a simplified representation of this formula. The formula for the SDC calculates the coefficient by taking twice the overlapping area and dividing it by the combined area of the two individual shapes. A coefficient of 1 indicates a perfect match in the registration, were both models are in the same position and orientation.

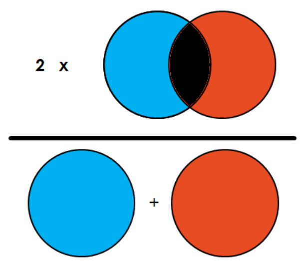

FIGURE 9: FORMULA FOR THE SØRENSEN-DICE COEFFICIENT, EXPRESSED IN FIGURES.

Geometry

The relevant geometry for an osteotomy was measured; the HKA in the frontal plane and the JLCA. In addition to these angles the HKA was be measured in the sagittal plane, and the rotation between tibia and femur was measured; the tibiofemoral rotation. To obtain accurate and repeatable measurements in 3D, the femur and tibia were first reoriented within the coordinate system. Within the coordinate system the mechanical axis formed the y-axis and the direction of the Akagi line is pointed forwards, forming the z-axis. This was done to make the measurements repeatable and similar to the clinical setting. The Akagi line has been shown to be the most reliable in showing rotational alignment (40). The femur and tibia are then placed within this coordinate system and the angles can be calculated. In Materialise 3-Matic (Materialise NV, Leuven, Belgium) anatomical markers were placed on each model. In MatLab these markers were used to place the models in the correct orientation and to automatically calculate the angles for each pair of 3D models.

Table 3 specifies the varies lines and axes that were constructed from the anatomical markers. Table 4 contains the different angles and their method of construction. Figure 10 shows the various lines and the angles constructed between the lines.

TABLE 3: THE VARIOUS LINES CONSTRUCTED IN THE 3D MODELS AND THE METHOD TO CONSTRUCT THE LINE.

Line	Markers
Mechanical axis	Centre of femoral head – midpoint articular surface distal tibia
Akagi line	Insertion point posterior cruciate ligament – medial border tibial tuberosity
Femoral mechanical axis (FMA)	Centre of femoral head – distal point trochlear groove
Tibial mechanical axis (TMA)	Midpoint lateral and medial eminence – midpoint articular surface distal tibia
Distal femoral condyles (DFC)	Distal point medial femoral condyle – distal lateral femoral condyle
Posterior femoral condyles (PFC)	Posterior point medial femoral condyle – posterior lateral femoral condyle
Tibial plateau	Medial point tibia plateau – lateral point tibia plateau
Posterior tibia plateau (PTP)	Posterior point medial tibia plateau – posterior point lateral tibia plateau

TABLE 4: THE ANGLES FORMED BY THE VARIOUS LINES FROM TABLE 1.

Angle	Measurement method
HKA frontal	Angle between FMA and TMA in frontal plane
HKA sagittal	Angle between FMA and TMA in sagittal plane
JLCA	Angle between DFC and tibia plateau in frontal plane
Tibiofemoral rotation	Angle between PFC and PTP in axial plane

Analysis

Statistical analysis was performed in SPSS Statistics 27 (IBM, Armonk, New York, USA). The inter-rater reliability and the intra-rater reliability were assessed with an intraclass correlation coefficient (ICC). The appropriate ICC test was chosen with the assistance of an article by Koo and Li (41). For the inter-rater reliability a two-way mixed effects ICC test was performed, based on a single rater measuring for absolute agreement. For the intra-rater reliability the same ICC test was be performed, but limited to the data of only rater 1. The ICC scores were interpreted according to the same article from Koo and Li (41). An ICC score under 0.50 indicates poor reliability, between 0.50 and 0.75 moderate reliability, between 0.75 and 0.90 good reliability, and a value above 0.90 indicates excellent reliability (41). The Pearson correlation was calculated between the angular measurements to analyse the differences between registered and reference 3D models. The mean absolute differences (MAD) of angular measurements and registration differences were calculated. The correlations between the two MADs were calculated with the Pearson correlation coefficient.

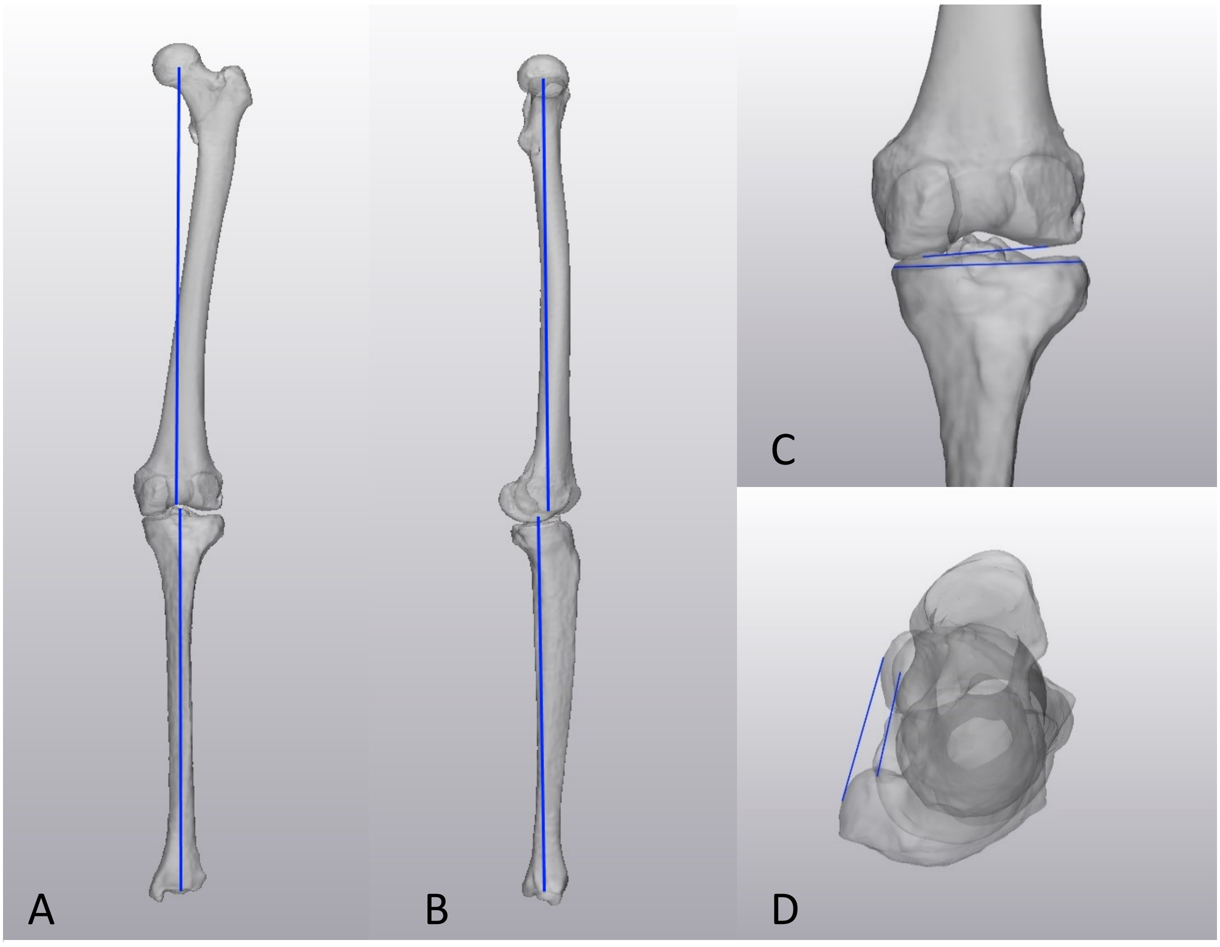

FIGURE 10: THE VARIOUS ANGLES THAT WERE MEASURED AND COMPARED BETWEEN REFERENCE MODEL AND REGISTERED MODEL. A) THE HIP-KNEE ANGLE IN THE FRONTAL PLANE, B) THE HIP-KNEE ANGLE IN THE SAGITTAL PLANE, C) THE JOINT-LINE-CONVERSION ANGLE, AND D) THE TIBIOFEMORAL ROTATION.

AUTOMATIC REGISTRATION

Materials

Registration algorithm

Automation of the 3D-2D registration was based on the same method used in the manual registration: minimizing the distance between contour of the anatomical 3D model and the contour of the bone in the WLR. The process was automated by use of an optimization algorithm. Such algorithms can help in finding the solutions for position and orientation where the distance between the two contours is minimal.

The constructed algorithm performed the registration in two steps: first a course but fast iteration, and second in a fine but slow iteration. The coarse registration was based on aligning the vectors between two sets of markers. Constructing the vectors between two sets of two markers for each bone, and aligning these vectors on the 3D model with the vectors on the x-ray will give a rough registration. The difference in length of the object in the X-ray and the length of the anatomical 3D model, was used to calculate the approximate depth position. This coarse step gives an initial solution for the optimization algorithm and helps in reducing the possible solutions needed to be investigated with the fine registration, therefore reducing calculation time. The markers were placed on anatomical landmarks visible on both the 2D WLR and the 3D model, Table 5.

TABLE 5: THE VECTORS THAT ARE ALIGNED FOR THE ROUGH REGISTRATION. VECTORS WERE CHOSEN AS TO HAVE A (MOSTLY) HORIZONTAL AND VERTICAL VECTOR.

Bone	Vector
Femur	Tip greater trochanter – Minor trochanter
	Tip greater trochanter – Femoral notch
Tibia	Later eminence – medial eminence
	Later eminence – Distal point medial malleolus

The fine registration used an optimization algorithm to find the final solution. Conventional registration algorithms work either two dimensional to two dimensional, or three dimensional to three dimensional. The most commonly used algorithm is the iterative closest point (ICP) algorithm. This algorithm is designed to iteratively minimize the differences between two sets of data and tries to find the translation and rotation matrices to align one dataset with the other dataset (42).

In a 3D-2D registration problem, the depth information is missing for the 2D image. In order to determine the correct depth position of the object or bone, the projection is of importance. As explained in the method for the manual registration, the projection changes depending on position between X-ray source and detector. Objects closer to the X-ray source will get a higher magnification than objects closer to the detector. This was used to find the correct Z-position in the space.

Because the projection changes for each possible position of the bone, the projection has to be updated for each iteration. Conventional ICP algorithms were therefore not usable for 3D-2D registration. An optimization algorithm was employed to find the orientation and position in which the difference between the contour of the 3D bone model and the bone in the WLR was minimal. The optimization algorithm was implemented in MatLab. MatLab has several optimization algorithms built-in, which assisted in implementing each method quickly and efficiently. With each new possible solution, the projection and the contour had to be calculated of the 3D model. An ICP registration is then able to register the contour of the bone in the WLR and the contour of the 3D model and find the corresponding points between the two shapes. This step was performed for each new possible solution to find the most optimal solution in which the contours aligned most. The pseudocode below describes the process as it was coded in MatLab. Further details are provided in the Appendix

```
Select 3Dmarkers on 3D model
Select 2Dmarkers on 2D image
Align vector between set of 3Dmarkers with vector of set of 2D markers
       repeat for at least two sets
Find size difference between vector 3D model and vector 2D model
Apply z-translation to make vectors same length
Input contour of bone in radiograph
Optimization algorithm
       find initial solution
       create perspective projection
       find contour of 3D model
       registrate using ICP algorithm                        Repeat
       find distance between silhouette and contour
       update optimization algorithm solution
Update 3D models with best solution
Save registered 3D models
```

Radiographs and 3D models

The (semi-)automatic registration was performed on a subgroup of the dataset used for assessing the manual registration. As the automation of the 3D-2D registration was approached as a proof-of-concept study, the registration was performed on the right side of 10 patients. More details on this dataset and the creation of the DRRs and 3D models can be found in previous paragraphs on the subject of manual registration. In summary: a group of CT scans from patients was used to construct digitally reconstructed radiographs (artificial X-rays) of the CT scan. Of the same CT scan, 3D models were segmented. When kept in the original position and using the same projection parameters as used for the creation of the DRR, the bones will align perfectly.

Design

With the data the registration algorithm was tested. In the algorithm three different optimization algorithms were included to find the solution to our optimization problem. Optimization algorithms try to find the solution to a formula while keeping the optimization metric (or cost function) as low as possible. Various optimization algorithms are available in MatLab. Below the optimization algorithms investigated for use are listed with a short explanation of their workings.

Genetic algorithm

The genetic algorithm was developed in the 1960s and 1970s. This algorithm generates an initial population of possible solutions. From this group a second generation is generated. Between each generation, the solutions will evolve based on principles from natural selection. This means the solutions will evolve through mutation, crossover and through a fitness evaluation of the outcome, in this case the distance from silhouette in the WLR to contour of the 3D model, the possible solutions are given a change of reproduction. The solutions with a better fitness function have a higher change of reproduction to the next generation (43).

Multi objective genetic algorithm

A multi objective genetic algorithm (MOGA) uses a regular genetic algorithm to optimize for multiple outcomes by constructing a pareto front. A pareto front are the found values for which either outcome 1 or outcome 2 is minimal. Figure 11 shows how the pareto front could look for an optimization. It is then up to the user to determine which outcome fits best for their use case. While the MOGA is not necessarily the best algorithm to use for this case, since outcome 1 (the registration error for the femur) and outcome 2 (the registration error for the tibia) don’t use any of the same input values, it is included because during preliminary testing it showed a good capability of finding the correct answers.

Surrogate algorithm

The surrogate algorithm is method useful for finding the solution to calculation-intensive and time-consuming functions (44). By sampling the function for a predetermined amount of solutions, the algorithm tries to create an easier to calculate approximation of the function in the form of a radial basis function (45). The approximation function gets occasionally checked against the original function and is updated.

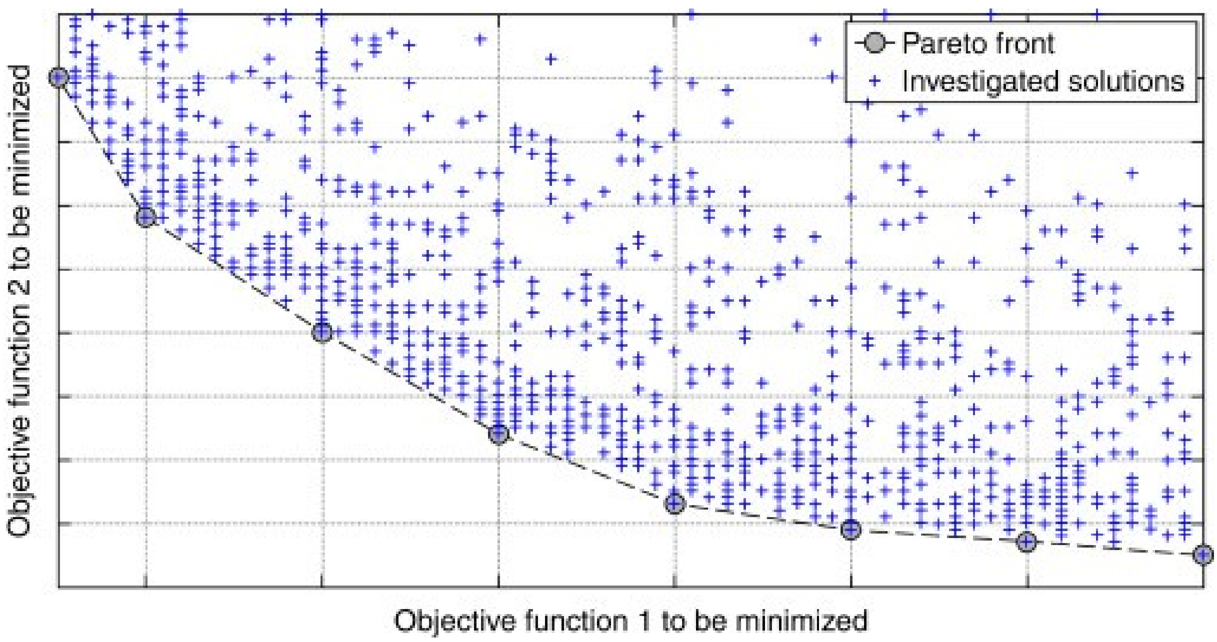

FIGURE 11: THE PARETO FRONT OF A MULTI OBJECTIVE GENETIC OPTIMIZATION IS THE LINE ACROSS THE OPTIMAL SOLUTIONS, FOUND ALONG ALL THE INVESTIGATED SOLUTIONS. THE USER WILL HAVE TO CHOOSE THE SOLUTION THAT FITS HIS USE CASE THE BEST (46).

Bounds and constraints

The optimization algorithm needs upper and lower bounds for the possible solutions, to limit the space in which the solution can be found. The following bounds were chosen:

- Rotation around x-axis: between -10 and 10 degrees
- Rotation around y-axis: between -30 and 30 degrees
- Movement in z-axis: between -100 and +100 millimetre

Next to the bounds, linear constraints were added to the optimization to ensure only valid answers were found. These were as follows:

- The centre of the lower 50mm of the distal femur and the centre of the upper 50mm op the proximal tibia could be no more than 20mm apart in the depth direction.
- The lowest vertex of the femur could not be any lower than the upper vertex of the tibia.

With the data available, the 3D models and the outline of the femur, the registration algorithms were tested. For the first 10 patients from the same dataset as for the manual registration, the right side of the patients were registered. The registration procedure was once performed with the outline of the bone in the WLR generated from the reference model, and once with the outline of the bone marked by the user. Generating the outline with the reference model helped in testing if the algorithm could reproduce the registration with perfect input data. The registrations were performed with the three different algorithms described above.

Measurements

The registered 3D models were measured with the same methods used in the measurements for the manual registration. These measurements are the Euclidean distance between each vertex of the models, and the difference between angular measurements performed on a pair of femoral and tibial 3D model. Angles used for realignment surgery planning were measured to assess the difference between registered models and reference models. Further details on how these angles were measured can be found in the paragraphs of the manual registration.

Analysis

Statistical analysis was performed in SPSS Statistics 27 (IBM, Armonk, New York, USA) in the same manner as for the manual registration. The reliability between different optimization algorithms was assessed with an intraclass correlation coefficient (ICC). The correct ICC test was chosen with the assistance of an article by Koo and Li (41). A two-way mixed effects ICC test was performed, based on a single rater measuring for absolute agreement. The ICC scores were interpreted according to the same article from Koo and Li (41). An ICC score under 0.50 indicates poor reliability, between 0.50 and 0.75 moderate reliability, between 0.75 and 0.90 good reliability, and a value above 0.90 indicates excellent reliability (41). The Pearson correlation was calculated between the angular measurements to analyse the differences between registered and reference 3D models.

RESULTS

MANUAL REGISTRATION

The registration error varied greatly between each rater. Figure 12 demonstrates this for one patient, where the colour indicates the Euclidean distance.

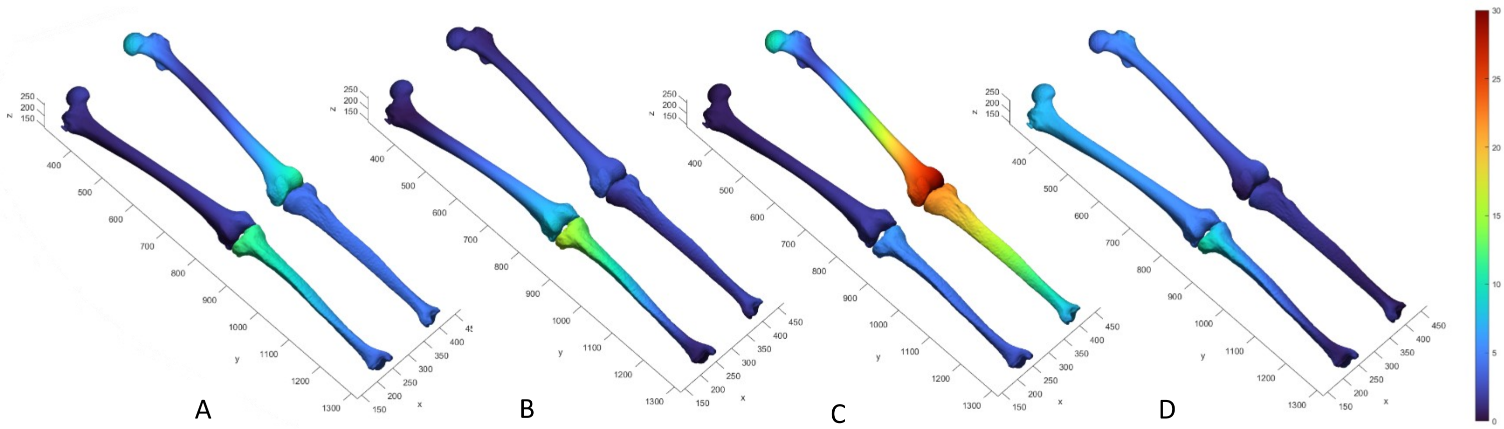

FIGURE 12: THE REGISTRATION ERROR IN THE XYZ-DIMENSION MASKED OVER THE 3D MODEL OF PATIENT 7. EACH PAIR OF 3D MODELS IS REGISTERED BY ONE OF THE RATERS. DARK BLUE COLOUR INDICATES GOOD REGISTRATION, WHILE RED INDICATES LARGE REGISTRATION ERROR. DISTANCES IN MILLIMETRES. A) RATER 1, FIRST REGISTRATION, B) RATER 1, SECOND REGISTRATION, C) RATER 2, D) RATER 3.

The average error after registration between the registered 3D models and the reference 3D models was between 6.26mm (± 4.42mm) in the XYZ-dimensions. When this error was split up in the XY- and the Z-components, the errors were between 0.89mm (± 0.39mm) in the XY-dimension and 6.10mm (± 4.47mm) in the Z-dimension. Table 6 shows the average error and standard deviations in the errors between the registered and reference models in both the femur and tibia.

TABLE 6: THE AVERAGE DISTANCE AND STANDARD DEVIATION BETWEEN THE CORRESPONDING POINTS FROM THE REGISTERED AND THE REFERENCE 3D MODEL

XYZ	Femur Right	Femur Left	Tibia Right	Tibia Left
Rater 1 (1st)	5.79 (± 4.55)	5.72 (± 3.22)	6.27 (± 4.09)	6.28 (± 4.47)
Rater 1 (2nd)	4.83 (± 2.86)	4.99 (± 3.75)	4.47 (± 3.19)	5.19 (± 3.31)
Rater 2	9.31 (± 5.03)	8.56 (± 5.70)	8.93 (± 4.91)	7.27 (± 5.93)
Rater 3	5.24 (± 4.00)	5.79 (± 4.04)	4.92 (± 2.70)	6.95 (± 4.11)

XY	Femur Right	Femur Left	Tibia Right	Tibia Left
Rater 1 (1st)	0.78 (± 0.40)	0.80 (± 0.27)	0.86 (± 0.28)	0.87 (± 0.47)
Rater 1 (2nd)	0.71 (± 0.26)	0.79 (± 0.29)	0.75 (± 0.27)	0.82 (± 0.26)
Rater 2	1.06 (± 0.31)	1.01 (± 0.40)	1.23 (± 0.47)	1.26 (± 0.51)
Rater 3	0.82 (± 0.30)	0.92 (± 0.44)	0.78 (± 0.28)	0.89 (± 0.39)

Z	Femur Right	Femur Left	Tibia Right	Tibia Left
Rater 1 (1st)	5.62 (± 4.50)	5.57 (± 3.30)	6.11 (± 4.09)	6.12 (± 4.45)
Rater 1 (2nd)	4.83 (± 2.84)	4.94 (± 3.75)	4.33 (± 3.20)	5.04 (± 3.30)
Rater 2	9.18 (± 4.99)	8.42 (± 5.90)	8.74 (± 4.90)	7.01 (± 5.92)
Rater 3	5.08 (± 3.98)	5.63 (± 3.98)	4.78 (± 2.90)	6.82 (± 4.10)

Figure 13 visualizes the average registration error from the four registrations for each patient. The trendline shows an increase in registration error over the course of the patient population. However, the R^2 for each patient is very low: 0.104 for the right femur, 0.095 for the left femur, 0.063 for the right tibia, and 0.022 for the left tibia.

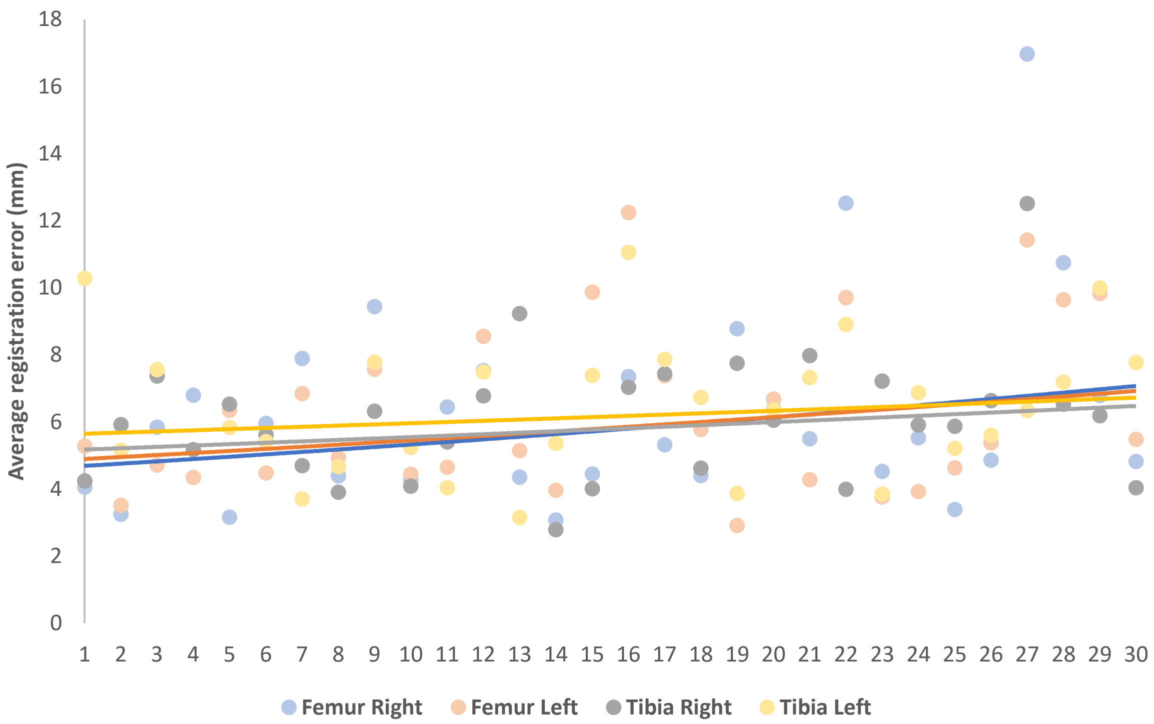

FIGURE 13: REGISTRATION ERROR IN XYZ-DIMENSIONS AVERAGED OVER THE REGISTRATIONS BY THE FOUR RATERS. THE TRENDLINE SHOWS IN INCREASE IN REGISTRATION ERROR OVER THE COURSE OF THE PATIENT POPULATION.

While registration errors increased mildly, registration times decreased, Figure 14. However, with a correlation factor of 0.179 the correlation between these two measures was weak. The average registration time was 6:49 minutes (± 2:00 minutes).

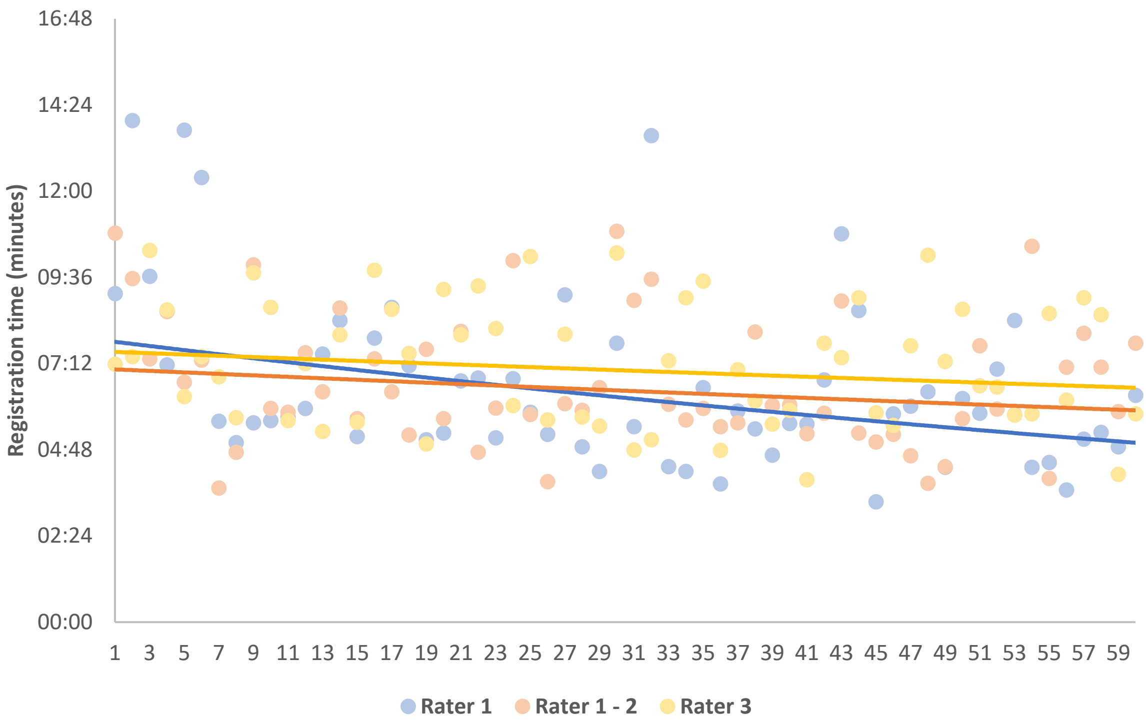

FIGURE 14: AVERAGE REGISTRATION TIME IN MINUTES FOR EACH SIDE OF A PATIENT. THE TRENDLINES SHOWS A DECREASE IN AVERAGE TIME NEEDED FOR A REGISTRATION FOR ALL RATERS. NO REGISTRATION TIMES WERE RECORDED BY RATER 2.

SDC were measured for all 3D models for the right pair of femur and tibia, left pair and total lower limbs. Figure 15 illustrates the distribution of the Dice scores all pairs of femur and tibia for each rater. The average SDC was 0.986 for both the right pair and left pair of femur and tibia, indicating a good fit in the frontal view.

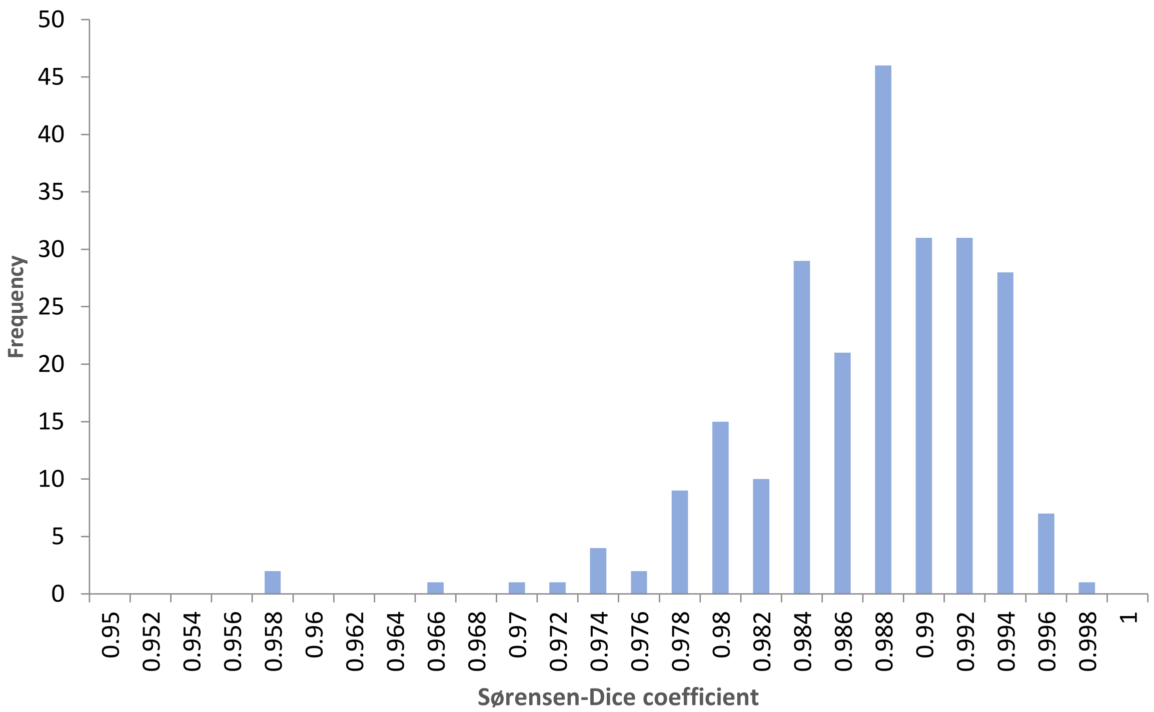

FIGURE 15: HISTOGRAM SHOWING THE DISTRIBUTION OF THE DICE SCORE FOR EACH PAIR OF FEMUR AND TIBIA. 240 PAIRS IN TOTAL WERE INCLUDED.

The angular differences between the reference 3D models and the registered 3D models, shown in Figure 16, illustrate how the distribution in change after registration is low for the HKA in the frontal plane and for the JLCA, but increases with the HKA in the sagittal plane and rotation. For the frontal HKA the average angular difference for the four raters combined was 0.60° (± 0.60°), for the sagittal HKA 1.63° (± 1.28°). For the JLCA this was 0.54° (± 0.64°), and for the rotation this was 1.69° (± 1.33°)

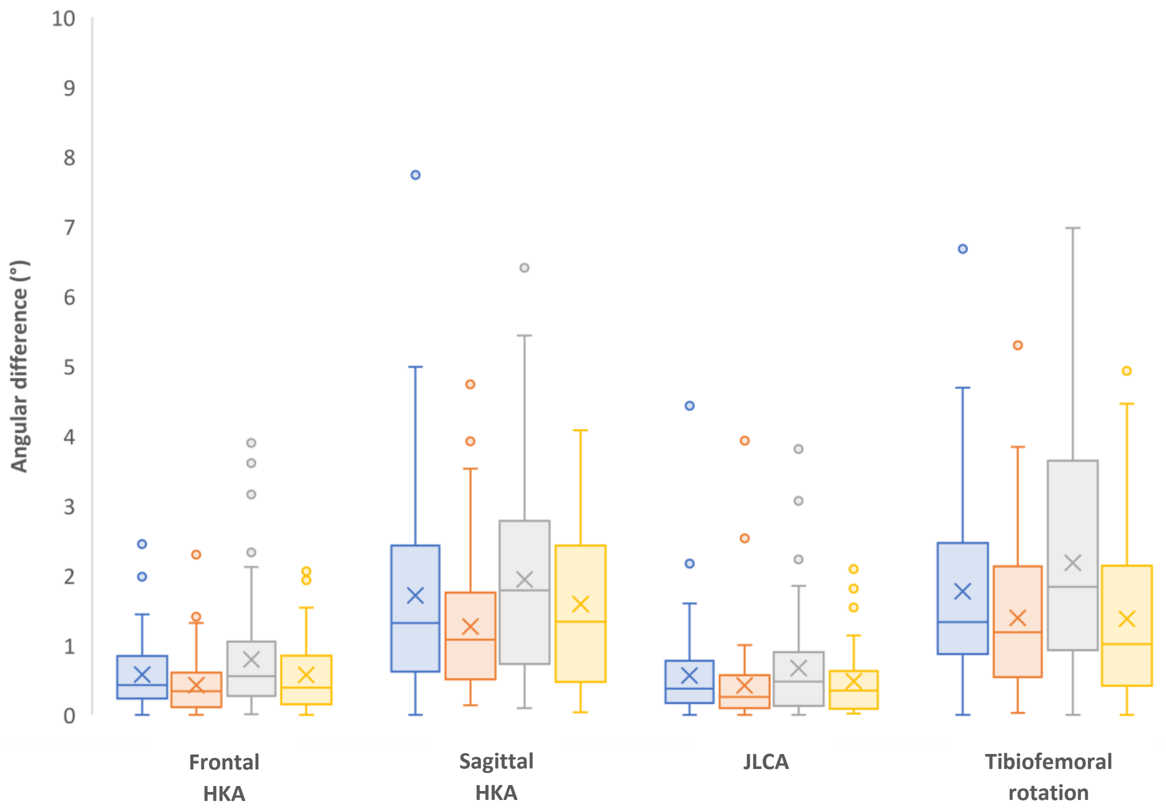

FIGURE 16: THE DISTRIBUTION OF THE DIFFERENCES IN MEASURED ANGLES BETWEEN REFERENCE AND REGISTERED MODELS FOR ALL RATERS. THE BLUE BOXPLOTS ARE RATER 1 (FIRST REGISTRATION), ORANGE = RATER 1 (SECOND REGISTRATION), GREY = RATER 2, YELLOW = RATER 3. HKA = HIP-KNEE-ANKLE ANGLE, JLCA = JOINT LINE CONVERSION ANGLE.

Inter-rater reliability between the various raters and intra-rater reliability between two measurements of rater 1 were measured for the different angles with an ICC. The found values for the interrater reliability are displayed in Table 7, while the values of the intra-rater reliability are displayed in Table 8.

TABLE 7: INTERRATER RELIABILITY BETWEEN THREE RATERS. HKA = HIP-KNEE-ANKLE ANGLE, JLCA = JOINT LINE CONVERSION ANGLE.

Angle	ICC
Frontal HKA	0.677 (95% CI 0.556 – 0.779, *p<0.001*)
Sagittal HKA	0.591 (95% CI 0.452 – 0.713, *p<0.001*)
JLCA	0.021 (95% CI -0.113 – 0.185, *p=0.382*)
Tibiofemoral rotation	0.625 (95% CI 0.493 – 0.740, *p<0.001*)

TABLE 8: INTRA-RATER RELIABILITY BETWEEN THE TWO MEASUREMENTS OF RATER ONE, WITH AN INTERMEDIATE PERIOD OF 2 WEEKS BETWEEN THE MEASUREMENTS. HKA = HIP-KNEE-ANKLE ANGLE, JLCA = JOINT LINE CONVERSION ANGLE.

Angle	ICC
Frontal HKA	0.749 (95% CI 0.612 – 0.842, *p<0.001*)
Sagittal HKA	0.540 (95% CI 0.332 – 0.697, *p<0.001*)
JLCA	0.292 (95% CI 0.043 – 0.507, *p=0.011*)
Tibiofemoral rotation	0.831 (95% CI 0.730 – 0.896, *p<0.001*)

For the interrater reliability the reliability between the raters for the frontal HKA, the sagittal HKA and the rotation were moderate, while the reliability in measurements for the JLCA was poor. The intra-rater reliability for the frontal HKA, sagittal HKA was moderate, the reliability for the JLCA was poor, and the reliability for the tibiofemoral rotation was good.

Correlation between the mean average distances of a pair of femur and tibia were calculated with the Pearson's correlation. The found values are displayed in Table 8.

TABLE 9: PEARSON CORRELATION COEFFICIENT BETWEEN AVERAGE DISTANCES PER PAIR OF FEMUR AND TIBIA AND ANGULAR DIFFERENCES. VALUES IN BOLD ARE SIGNIFICANT (P<0.01). HKA = HIP-KNEE-ANKLE ANGLE, JLCA = JOINT LINE CONVERSION ANGLE.

	Frontal HKA	Sagittal HKA	JLCA	Tibiofemoral rotation
Distance XYZ	**0.312**	**-0.239**	0.091	-0.098
Distance XY	**0.185**	-0.780	0.026	-0.039
Distance Z	**0.311**	**-0.239**	0.091	-0.098

The Pearson correlation was used again for measuring the agreement between the angles measured in the reference models and the registered models. For the frontal HKA a correlation of 0.782 (p<0.01) was found, for sagittal HKA a correlation of 0.708 (p<0.01), for the JLCA a correlation of 0.162 (p=0.012), and for the tibiofemoral rotation a correlation of 0.774 (p<0.01).

AUTOMATIC REGISTRATION

The automatic registration has produced varying results between each optimization algorithm. This is illustrated when the registration errors of the different optimization methods of a single patient are compared with each other (Figure 17), and this is further show in the three tables, which show the average distance error for each case, Table 10, 11 and 12.

The registration results varied between each optimization method. The mean registration error was 30.10mm for the genetic algorithm (GA), 12.83mm for the multi objective GA, and 33.81mm for the surrogate algorithm.

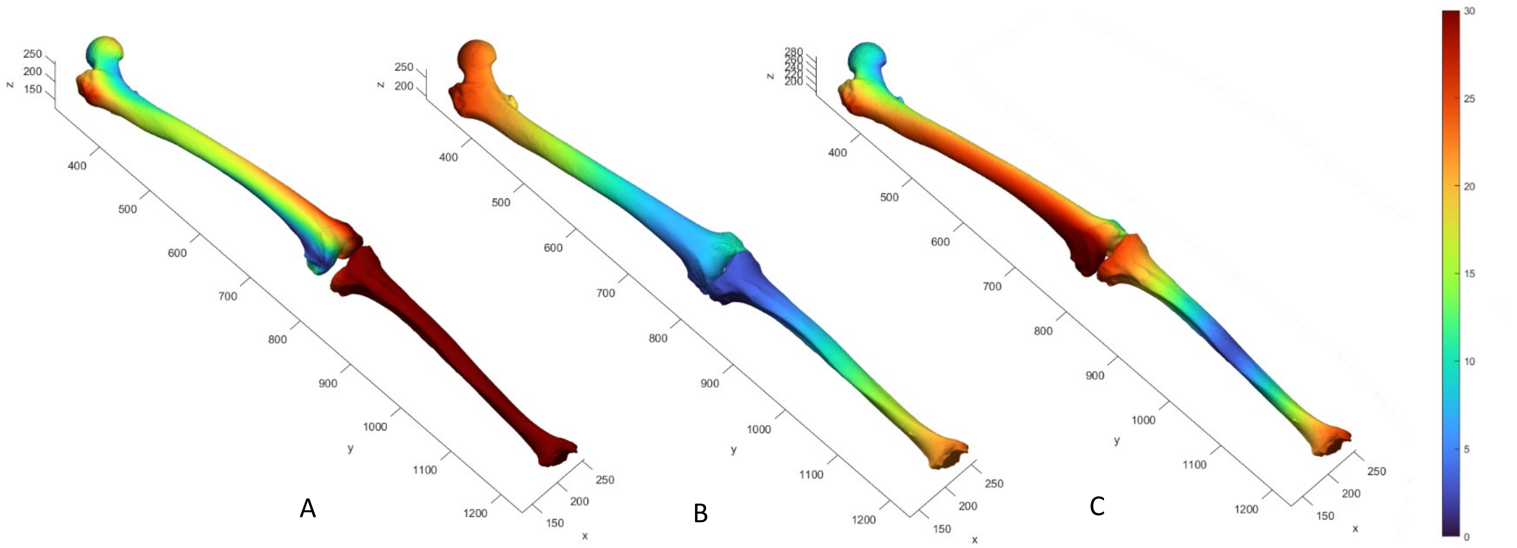

FIGURE 17: THE REGISTRATION ERROR IN THE XYZ-DIMENSION MASKED OVER THE 3D MODEL OF PATIENT 1. EACH PAIR OF 3D MODELS IS REGISTERED BY ONE OF THE OPTIMIZATION ALGORITHMS. DARK BLUE COLOUR INDICATES GOOD REGISTRATION, WHILE RED INDICATES LARGE REGISTRATION ERROR. DISTANCES IN MILLIMETRES. A) GENETIC ALGORITHM, B) MULTI OBJECTIVE GENETIC ALGORITHM, C) SURROGATE ALGORITHM

Average time to complete the registrations was 50 minutes (range 13-76 min) for the GA, 66 minutes (range 14-93 min) for the multi objective GA, and 19 minutes (range 4-45 min) for the surrogate algorithm optimization.

The Sørensen-Dice coefficients acquired by the different optimization algorithms, shown in Figure 18, ranged between 0.531 and 0.986. The GA achieved the worst in general, with an average SDC of 0.850 over the 10 test subjects. The multi objective GA got an average SDC of 0.949, while the surrogate algorithm got an average SDC of 0.934.

The angular differences, Figure 19, show how the automatic registration mainly struggled with the tibiofemoral rotation. The angular differences are further defined in Table 13.

TABLE 10: THE AVERAGE REGISTRATION ERROR BETWEEN THE REGISTERED MODEL AND THE REFERENCE MODEL IN MILLIMETRE FOR THE GENETIC ALGORITHM. ERRORS GIVEN IN THE XYZ-DIMENSION, XY-DIMENSION, AND IN THE Z-DIMENSION

XYZ	Femur	Tibia	XY	Femur	Tibia	Z	Femur	Tibia
1	14.78 (±8.32)	52.32 (±24.39)		7.88 (±4.87)	8.64 (±1.69)		10.81 (±9.22)	51.34 (±24.86)
2	11.90 (±5.78)	12.35 (±0.94)		5.94 (±3.81)	3.79 (±0.76)		9.10 (±6.51)	11.70 (±1.21)
3	13.22 (±5.98)	10.75 (±4.75)		5.61 (±3.60)	3.81 (±2.39)		11.02 (±6.69)	9.50 (±5.25)
4	27.08 (±20.27)	6.13 (±1.93)		20.22 (±19.89)	3.12 (±0.50)		12.45 (±13.58)	5.13 (±2.25)
5	79.16 (±18.74)	94.97 (±8.42)		25.17 (±19.61)	6.94 (±1.47)		73.03 (±16.29)	94.69 (±8.50)
6	7.42 (±4.21)	8.44 (±5.15)		2.54 (±1.51)	1.34 (±0.76)		6.59 (±4.55)	8.20 (±5.30)
7	32.77 (±10.47)	44.21 (±14.84)		7.36 (±3.79)	12.91 (±17.97)		31.75 (±10.33)	39.54 (±11.05)
8	45.57 (±10.92)	33.52 (±8.47)		18.04 (±9.86)	21.25 (±3.07)		40.69 (±10.84)	23.69 (±13.15)
9	30.73 (±16.39)	7.20 (±0.67)		11.34 (±1.80)	6.18 (±1.03)		26.13 (±19.96)	3.51 (±0.90)
10	27.48 (±18.44)	42.09 (±9.65)		2.97 (±1.99)	2.41 (±0.48)		27.10 (±18.65)	42.01 (±9.67)
Mean	29.01 (±11.95)	31.20 (±7.92)		10.71 (±7.07)	7.04 (±3.01)		24.87 (±11.66)	28.93 (±8.21)

TABLE 11: THE AVERAGE REGISTRATION ERROR BETWEEN THE REGISTERED MODEL AND THE REFERENCE MODEL IN MILLIMETRE FOR THE MULTI OBJECT GENETIC ALGORITHM. ERRORS GIVEN IN THE XYZ-DIMENSION, XY-DIMENSION, AND IN THE Z-DIMENSION

XYZ	Femur	Tibia	XY	Femur	Tibia	Z	Femur	Tibia
1	13.44 (±7.47)	8.64 (±8.22)		3.57 (±1.88)	1.65 (±0.69)		12.28 (±8.33)	8.07 (±8.60)
2	4.35 (±2.85)	4.19 (±2.12)		0.89 (±0.30)	0.73 (±0.38)		4.05 (±3.13)	4.09 (±2.16)
3	7.24 (±5.09)	8.99 (±4.07)		0.79 (±0.43)	4.19 (±2.60)		7.12 (±5.18)	7.30 (±4.45)
4	27.50 (±20.29)	12.62 (±1.49)		20.14 (±20.05)	1.05 (±0.23)		13.21 (±13.64)	12.57 (±1.50)
5	30.99 (±19.50)	5.11 (±1.31)		21.55 (±19.47)	1.27 (±0.60)		16.99 (±14.45)	4.90 (±1.33)
6	13.55 (±6.02)	4.49 (±1.08)		3.01 (±1.21)	1.14 (±0.50)		12.97 (±6.40)	4.31 (±1.11)
7	20.50 (±6.37)	19.40 (±18.47)		5.65 (±2.26)	14.49 (±19.67)		19.33 (±7.10)	9.61 (±5.30)
8	16.50 (±9.80)	7.11 (±3.11)		5.16 (±1.95)	2.95 (±1.50)		14.83 (±10.87)	6.12 (±3.43)
9	15.83 (±8.18)	17.51 (±4.11)		6.51 (±2.63)	1.77 (±0.87)		13.95 (±8.58)	17.40 (±4.14)
10	12.04 (±5.37)	6.57 (±0.59)		1.83 (±0.96)	0.52 (±0.26)		11.80 (±5.50)	6.55 (±0.59)
Mean	16.19 (±9.09)	9.46 (±4.46)		6.91 (±5.11)	2.98 (±2.73)		12.65 (±8.32)	8.09 (±3.26)

TABLE 12: THE AVERAGE REGISTRATION ERROR BETWEEN THE REGISTERED MODEL AND THE REFERENCE MODEL IN MILLIMETRE FOR THE SURROGATE ALGORITHM. ERRORS GIVEN IN THE XYZ-DIMENSION, XY-DIMENSION, AND IN THE Z-DIMENSION

XYZ	Femur	Tibia	XY	Femur	Tibia	Z	Femur	Tibia
1	19.64 (±7.35)	19.60 (±6.97)		5.27 (±3.40)	2.22 (±1.46)		18.40 (±7.87)	19.38 (±7.10)
2	32.21 (±5.33)	41.93 (±6.58)		4.49 (±1.33)	1.68 (±0.63)		31.85 (±5.44)	41.89 (±6.60)
3	14.51 (±9.70)	11.99 (±7.06)		3.92 (±0.59)	4.63 (±2.44)		13.42 (±10.43)	10.73 (±7.13)
4	39.36 (±17.91)	13.71 (±2.36)		21.22 (±19.44)	1.36 (±0.22)		29.30 (±13.55)	13.64 (±2.38)
5	35.24 (±16.51)	11.74 (±7.19)		21.97 (±19.86)	1.19 (±0.61)		23.92 (±8.07)	11.55 (±7.36)
6	56.62 (±7.92)	66.91 (±11.12)		5.97 (±2.62)	5.47 (±0.78)		56.24 (±7.92)	66.66 (±11.21)
7	44.35 (±10.77)	31.84 (±20.44)		6.91 (±1.66)	13.54 (±17.68)		43.71 (±11.07)	26.05 (±16.03)
8	20.92 (±12.46)	22.52 (±13.38)		3.85 (±2.37)	5.07 (±3.11)		20.25 (±12.74)	21.46 (±13.80)
9	80.01 (±2.27)	70.39 (±4.06)		7.61 (±0.60)	6.93 (±0.72)		79.65 (±2.32)	70.04 (±4.10)
10	17.93 (±6.02)	24.68 (±2.33)		3.63 (±1.45)	1.70 (±0.44)		17.46 (±6.16)	24.61 (±2.34)
Mean	36.08 (±9.63)	31.53 (±8.15)		8.48 (±5.33)	4.38 (±2.81)		33.42 (±8.56)	30.60 (±7.81)

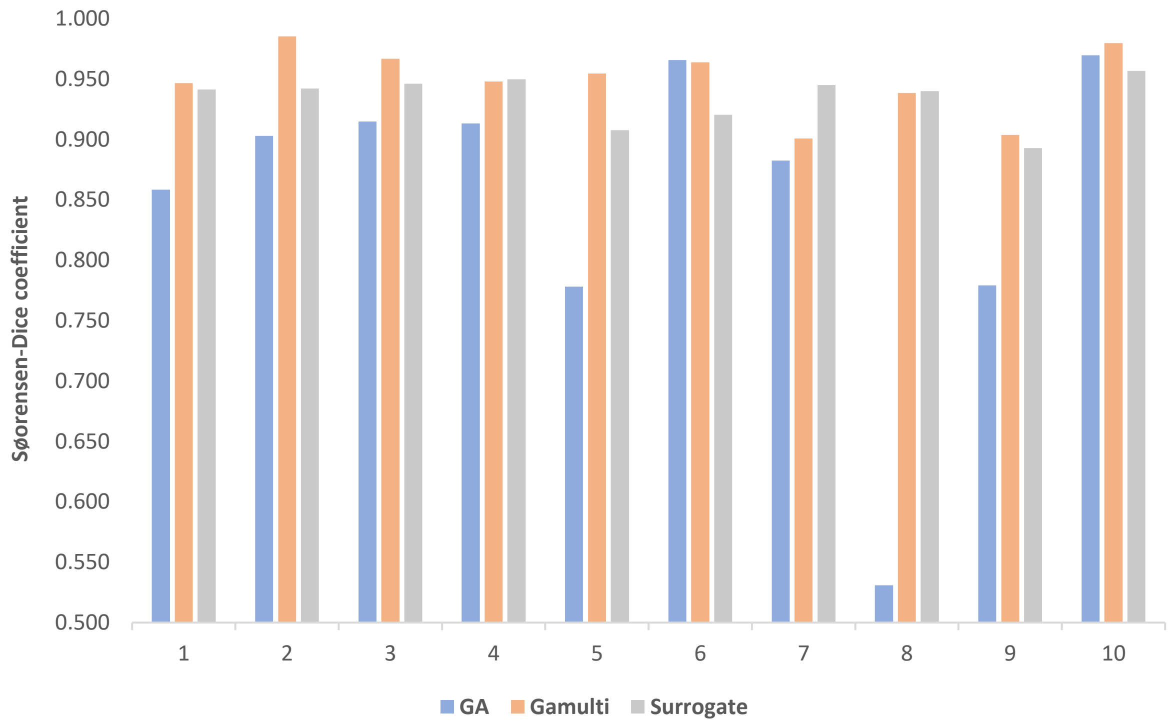

FIGURE 18: THE SØRENSEN-DICE COEFFICIENTS PER PAIR OF FEMUR AND TIBIA FOR EACH PATIENT FOR THE VARIOUS OPTIMIZATION ALGORITHMS

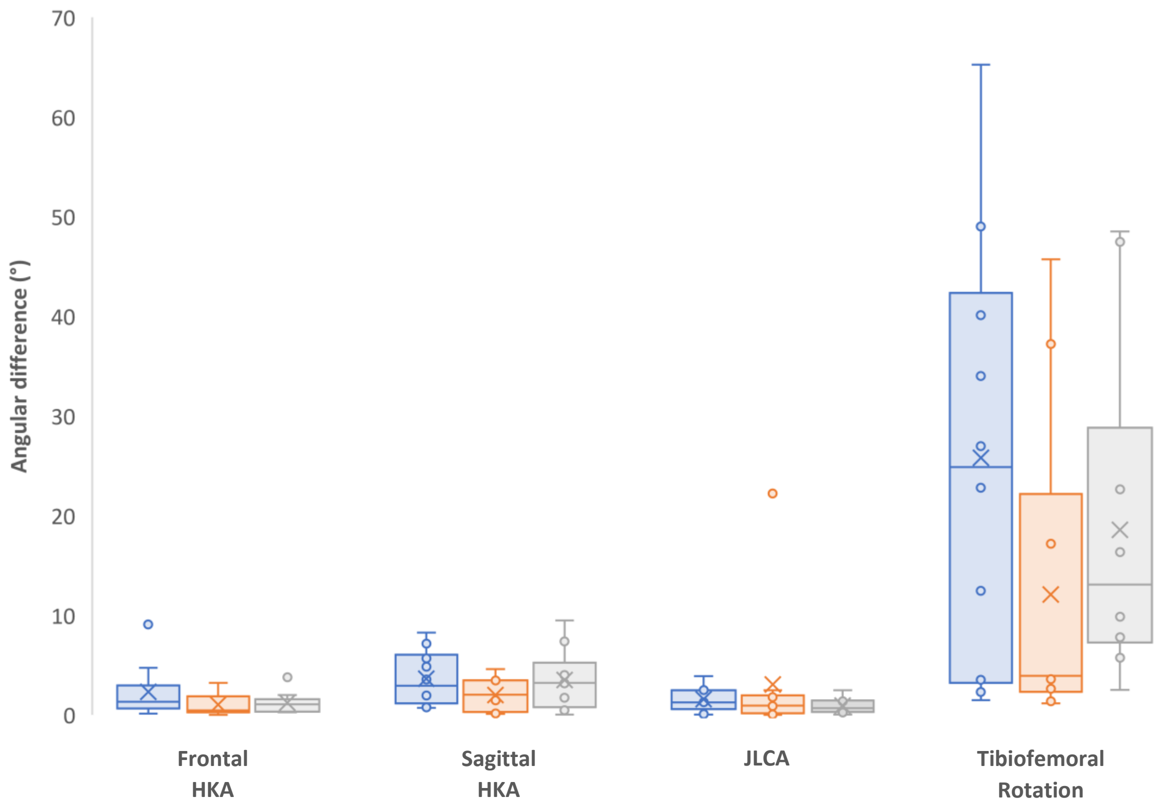

FIGURE 19: THE DISTRIBUTION OF THE DIFFERENCES IN MEASURED ANGLES BETWEEN REFERENCE AND REGISTERED MODELS FOR ALL RATERS. THE BLUE BOXPLOTS = GA, ORANGE = MULTI OBJ. GA, GREY = SURROGATE ALGORITHM. HKA = HIP-KNEE-ANGLE, JLCA = JOINT LINE CONVERSION ANGLE.

TABLE 13: THE MEAN ABSOLUTE ANGULAR ERRORS AFTER REGISTRATION, COMPARED TO THE REFERENCE MODELS. HKA = HIP-KNEE-ANKLE ANGLE, JLCA = JOINT LINE CONVERSION ANGLE.
*PATIENT 7 WAS EXCLUDED FROM DUE TO BEING LARGE OUTLIER

	Frontal HKA	Sagittal HKA	JLCA	Tibiofemoral rotation
GA	2.32° (±2.59°)	3.65° (±2.58°)	1.57° (±1.18°)	25.79° (±20.48°)
Multi obj. GA	1.04° (±1.10°)	1.99° (±1.46°)	0.93° (±0.77°) *	12.09° (±15.43°)
Surrogate	1.25° (±0.99°)	3.50° (±2.89°)	0.93° (±0.74°)	18.57° (±15.75°)

The Pearson's correlation was calculated between reference angles and the measured angles from the different algorithms. These values are displayed in Table 14.

TABLE 14: PEARSON CORRELATION COEFFICIENT BETWEEN ANGULAR MEASUREMENTS ON REGISTERED MODELS AND REFERENCE MODELS. HKA = HIP-KNEE-ANKLE ANGLE, JLCA = JOINT LINE CONVERSION ANGLE.

	Frontal HKA	Sagittal HKA	JLCA	Rotation
GA	0.206 (p = 0.567)	-0.086 (p = 0.814)	0.270 (p = 0.450)	0.055 (p = 0.880)
Multi obj. GA	0.802 (p = 0.005)	0.344 (p = 0.330)	-0.363 (p = 0.302)	0.282 (p = 0.430)
Surrogate	0.491 (p = 0.150)	-0.104 (p = 0.774)	0.268 (p = 0.453)	0.233 (p = 0.518)

The graphs and tables above show the results when using reference input. When the contour is drawn by the user, the average registration error using the GA is 42.04mm for femora and 43.05 for the tibia, the registration error is 16.05mm for femora and 12.75mm for tibiae when using the multi objective GA, and with the surrogate algorithm the mean registration error is 30.68mm and 35.76mm for femur and tibiae respectively.

Comparing the angular measurements acquired with either the reference contour input or the user input gave the following correlation: for the GA 0.859 (p<0.001), for the multi objective 0.988 (p<0.001) and for the surrogate algorithm 0.967 (p<0.001).

DISCUSSION

Manual registration

The aim of this study was to investigate the possibility of manual 3D-2D registration for creating weight-bearing 3D models of the lower limb. With the use of dedicated software for 3D-2D registration we were able to recreate models with good accuracy in the frontal plane, but results were less accurate in the sagittal plane. With the results we were able to show that manual registration can be used to perform registration and the registration is accurate in terms of angular measurements currently in use for preoperative osteotomy planning.

The registration errors were mostly present in the sagittal plane, with the average error in this direction being 6.10mm. The registration errors were significantly lower in the XY-dimension, with the average error being only 0.89mm. This can be explained by the use of AP radiographs, which only contain information in the XY-dimension. The Sørensen-Dice coefficients confirmed the low margin of error in registration, with a high coefficient of 0.986. The high SDC indicates a good match between the projected shadow of the 3D anatomical models and the WLR. However, the SDC needs to approach a coefficient of 1 for the other registration error measurements to be considered accurate. Seemingly small discrepancies between the alignment of 3D model and the WLR can results in relatively large errors in registration.

More clinically relevant are matching geometrical angles, used in clinical care for diagnosis and pre-operative planning. Comparably to the error assessments of the distances, the registration results are more accurate in the XY-dimension than in the Z-dimension. Measured lower limb geometry angles of the 3D-2D registrations in the frontal plane are very accurate, compared to the reference models. The absolute mean difference of the frontal HKA was 0.60° and 0.54° for the JLCA. Analysis of the geometry in the transversal and sagittal plane resulted in higher errors. Mean absolute angular differences for the sagittal HKA were 1.63° and 1.69° for the tibiofemoral rotation.

Manual 3D-2D registration time was on average 6:49 minutes per pair of femur and tibia. The average registration time decreased over the course of the patient group. This could indicate an increase in raters 3D-2D registration skills as progressed through the test subjects. However, the registration errors increased over the patient population. The increase in registration error and decrease in registration time correlated, even though this correlation was weak. This could indicate that taking more time could result in more accurate 3D-2D registrations.

Inter-rater reliability was moderate for all angles except the JLCA, for which the reliability was poor. Intra-rater reliability was moderate to good for all angles, except for the JLCA again, where the intra-rater reliability was poor. The intra-rater reliability was however better for the frontal HKA, JLCA and the tibiofemoral rotation, while only slightly decreasing for the sagittal HKA. This would suggest that using the same rater would produce more consistent results than using different raters each time. Using the same rater could improve reliability of the performed registration.

Pearson correlation between the geometrical measurements on the reference models and the registered models correlated moderately for the frontal HKA, sagittal HKA and tibiofemoral rotation, while the JLCA correlated poorly. This could be explained at the smaller range of the normal JLCA, which is between 0° and 2°. This normal range is smaller than for the other angles, therefore a variation in the measured angles will sooner give a worse correlation.

3D-2D registration performance was not significantly different between the 3 raters, this means that with good instructions and practice users can achieve similar results. By using multiple raters we were able to show that the registration error was similar between the different raters. This is important as the results do not rely on the user of the software, and with good instructions and training multiple users can achieve similar results.

For use of the of the registered models in clinical settings, results of angular measurements must not differ significantly from results achievable with the current golden standard, measurements on 2D radiographs. Nguyen et al found that on 2D radiographs, the variation in angles measured by different raters was between 0.5-1° (27). The mean error of the frontal HKA and the JLCA fall within this range. The JLCA angles had however poor correlation between reference measurements and measurements on the registered models.

Automatic registration

The aim of this study was to investigate the possibility of 3D-2D registration using an optimization algorithm. Registration using a multi objective genetic algorithm resulted in the highest accuracies in both absolute distance errors and angular errors.

The accuracy achieved with each of the optimization algorithm varied from patient to patient. Mean registration distance error was lowest for the multi objective GA with 12.83mm, while the GA achieved a mean distance error of 30.10mm and the surrogate algorithm a mean error of 33.81mm.

The high registration errors also translated to the Sørensen-Dice coefficients, with the SDC of the multi objective GA being the highest at 0.949, compared to the average SDC of the Surrogate algorithm of 0.934 and 0.850 for the GA. However, the SDC is not indicative of an accurate registration. As discussed earlier, the SDC needs to approach a coefficient of 1 to achieve accurate registration results. The results achieved with the optimization algorithms confirm this, as the relatively high SDC of 0.934 still results in poor registration results.

Of the three optimization methods, the surrogate algorithm performed the 3D-2D registration the quickest. The mean registration times was 19 minutes. However, this could be up to 45 minutes in some of the cases but also as quick as 4 minutes. Registration time of the multi objection GA and GA was more consistent, the mean time respectively being 66 minutes and 50 minutes. The algorithm was run on a personal computer. Utilizing dedicated hardware, with high core count CPUs, can reduce the calculation time as more calculations can be processed simultaneously.

For the 3D-2D registrations the contour of the femur and tibia in the WLR was derived from the 3D model to ensure that perfect input data was available for the registration and optimization algorithm. The algorithm was also tested with user input as data. The registration results between the reference input and the user input correlated very well, especially for the multi objective GA and the surrogate algorithm, with a Pearson correlation reaching close to 1. The achieved accuracies therefore did not differ significantly with the input. User input can reach the same accuracies as the reference input with the current registration algorithms. A shortcoming with user input for marking of the bone contour in the radiograph, is the introduction of inter-rater variability. Manual contour marking introduces variations between users and therefore variations in the registration results. An automatic method for segmentation of the bone contour from the radiograph will reduce the time, while likely achieving more consistent registrations. BoneFinder software (version 1.3.4a, Centre for Imaging Sciences, The University of Manchester, Manchester, United Kingdom) was investigated to assist in this task (47,48). This software, at the time of writing, only segments the proximal femur and the knee joint. This made BoneFinder not suitable, as large parts of the bone contour would not be included for registration.

Additionally, the segmentation by BoneFinder required extensive adjustments to accurately mark the contour of the bone, undoing the benefit of an automatic segmentation. Reliable and automatic segmentation of the bones on 2D radiographs could be beneficial for the 3D-2D registration problem.

The same shortcoming exists for the anatomical 3D models. Accurate segmentation of the bone out of the CT scan is crucial for an accurate registration result. Despite using dedicated software for bone segmentation from CT scans, inter-rater variability will always be present. Thresholding segmentation requires manual post processing to acquire a valid and usable 3D model. This introduces variations in the model of up to 0.6mm (49). Differences in anatomical 3D models affect the bone contour and therefore the registration outcome.

Clinical relevance

The aim of this project was to create weight-bearing 3D models out of CT scans and WLRs. This was realized by performing manual 3D-2D registration, with good accuracies in the frontal plane. Additionally, automation of the 3D-2D registration process was investigated. This resulted in lower accuracies in all planes.

From previous research, we know that in the current gold standard for osteotomy planning using 2D radiographs, the error between measurements from different raters is 0,5-1,0° (27,50). Accuracies of the HKA and JLCA after manual registration were comparable. This indicates that manually created weight bearing 3D models do not exceed the errors currently observed in clinical care.

The accuracies achieved in the sagittal plane and the transversal plane are worse, and the range in errors is higher than observed on 2D radiographs. This indicates that alignment measurements can be accurately performed on registered 3D models in the frontal plane. However, measurements in the sagittal and transversal plane cannot be accurately performed on the registered anatomical 3D models. For osteotomies in patients without rotational deformities, the use of registered 3D models does not provide additional information and benefits, compared to the current standard of pre-operative planning using 2D WLRs. However, for patients with rotational deformities the use of the registered 3D models can still provide additional benefits. In current practice, non-weight bearing 3D models are used. Registered weight-bearing 3D models could provide additional information in the sagittal plane and the frontal plane on rotational deformities of the knee and slope measurements. However, further investigation has to be conducted to assess the added value for these kinds of defects.

Manual 3D-2D registration of femur and tibia has not been performed before in research. Most of the research focusses on automated registration methods using fluoroscopy images (51–53). One of the main challenges in this kind of research is the acquisition of a dataset that can be used for validation of the registration. By using DRRs we were able to generate the required dataset and accurately validate the registration. Similar studies use small datasets consisting of only a few patients and are not able to validate their results on larger patient groups. This study is therefore an important step in getting manual 3D-2D registration validated for clinical applications. The registered models could also aid further research for gait or motion analysis and kinematics of the knee, where the weight-bearing aspect of models is important

Since no datasets were available combining WLRs with femoral and tibial 3D models in the exact same position, the use of an artificially created dataset was necessary to conduct this research. The artificial WLRs, the digital reconstructed radiographs, are limited in resolution by the CT scan. The CT scans had pixel sizing of 0.7mm x 0.7mm in the XY-direction and slice thickness ranging between 0.6 and 1.0mm. This resulted in a spatial resolution of approximately 0.7 line pairs per millimetre (lp/mm). A radiograph can reach a higher spatial resolution of 3 lp/mm (54). Real WLRs have therefore higher spatial resolution and bone contour and structures are better visible. This might produce more accurate registration results. Future research should therefore focus on creating a dataset using real WLRs. This could be possible with the use of sawbones. In the recommendations more details will be given.

This research performed the 3D-2D registrations based on only one AP radiograph. By limiting ourselves to only one direction, less information was available regarding the depth position and orientation of the lower limb. This limitation was chosen as in the clinical setting per protocol only the single AP radiograph is made. In most clinical centres only AP WLRs are available, making the proposition of this project implementable in most clinics. A recent study by Roth et al. performed an automatic 3D-2D registration of femur and tibia with images gathered by an EOS imaging system (55). This system is capable of acquiring a frontal and sagittal radiograph simultaneously. Stereo radiography is able to give depth information of the subjects. Therefore, their 3D-2D registration was easier to perform. They were able to achieve an average registration error of 1.1mm. The depth information does not have to be gathered solely from the perspective projection, giving more accurate results.

Recommendations

In the clinical setting the WLRs are made from three x-rays stitched together (27). This creates a perspective that is different from the single image projection used in this research. When creating a dataset of real WLRs, this differing projection will be applied to the WLR. Further assessments need to be performed on how this changes the registration process. These changes in the projection will also have to be implemented in the registration software. Differing projection between the WLR and the registration software can result in inaccurate registration.

Further research has to be performed with the 3D-2D registration software to test the ability of 3D-2D registration on real WLRs. As mentioned earlier, the creation of dataset consisting of WLRs and anatomical 3D models is difficult. In this study we were limited by having to perform the registration on DRRs. Testing the registration on real WLRs is a crucial step in getting further validation of the registration results. Creation of such a database could be performed by fixating radiopaque Sawbones in a frame. Anatomical models could then be created to mimic the lower limb. Applying radiopaque markers on the frame, and accurate measurements of projection parameters, can aid in acquiring the true position of the 3D models in the WLR. With real WLRs the accuracy of the registration could further improve. This could be especially important for the registration accuracy in the sagittal plane.

The automatic registration will have to be improved to be clinically viable. This study included three optimization algorithms, however several other optimization algorithms are available for implementation in MatLab. Preliminary testing indicated that the included algorithms would perform best in 3D-2D registrations. Of the included optimization algorithms, the multi objective GA was the most accurate while the surrogate algorithm was the fastest. Of the three algorithms included in this research, we recommend to only investigate the multi objective GA and the surrogate algorithm further for automation of the 3D-2D registration. These two algorithms show the best potential for creating a fast and reliable registration algorithm.

The automatic 3D-2D registration algorithm included next to the optimization algorithm a proven ICP algorithm (56,57). The ICP algorithm was responsible for XY-translation and rotation around the Z-axis. The rationale behind the inclusion of the ICP algorithm was to reduce calculation time by the optimization algorithm and reduce the number of variables. However, the ICP algorithm could be replaced by the optimization algorithm. The optimization algorithm will then have to optimize for more variables, but results could be more predictable. It is unknown if this would reduce registration time or registration accuracy.

Various upper and lower bounds and non-linear constraints were implemented in the algorithm. The bounds decrease the search area for the solution, and therefore search time. The constraints were necessary to ensure only realistic answers were found. Without these constraints, the distal femur and the proximal tibia would often not align in the sagittal plane. However, the non-linear constraints made the optimizations multiple orders of magnitude slower. Possible solutions have to be discarded as they do not meet the constraints. This increases the time needed for the algorithm to find viable solutions, and to optimize for these solutions. Further optimization of the constraints could decrease computation time and potentially decrease registration errors. The constraints could be more tightly integrated in the algorithm, to prevent double calculations.

The anatomical models used in this project were kept in their original resolution. Some of these models consist of up to 80.000 vertices. This increased the computational time, in order to recalculate the position of all the vertices for every step in the registration process. However, a big portion of the vertices in the model are not needed for the registration and only slow down the optimization. We predict that the registration time can be reduced significantly by implementing a multi-resolution approach to the optimization. Separating the registration in multiple steps, and increasing the resolution from stage to stage reduces to the calculation time while keeping accuracy the same.

By using the DRR approach for the research, more WLRs can be created from ordinary lower limb CT scans. This can be implemented in an artificial intelligence (AI) approach, using machine learning or deep learning. These methods would require large databases to learn from. Machine learning or deep learning has the potential to create a method that is faster and more accurate. However, depth information is still unavailable in the single view 2D approach used in this study, and it is not known how well an AI approach would be able to solve the 3D-2D registration.

Newer and more advanced imaging modalities must be considered. The article by Roth et al. shows that the addition of a second radiograph by using of an EOS system greatly improves the accuracy of the registration. This, in turn, can improve accuracy of the osteotomy planning and the surgical results. Therefore, the additional costs of such a system have to be strongly considered.

CONCLUSION

In this study the ability of a manual and a semi-automatic method of 3D-2D registration for the creation of weigh bearing 3D models of the lower limbs was investigated. The manual method produced accurate results in the frontal plane. However, results were not accurate enough in sagittal and axial plane for clinical use. The automatic registration, tested using three different optimization algorithms, achieved less accurate results than the manual registration. The automatic 3D-2D registration in its current form is not useable and needs further optimization to decrease registration errors and to speed up the process.

BIBLIOGRAPHY

1. Hirschmann MT, Müller W. Complex function of the knee joint: the current understanding of the knee. Knee Surgery, Sport Traumatol Arthrosc. 2015;23(10):2780–8.

2. Becker R, Kopf S, Karlsson J. Loading conditions of the knee: What does it mean? Knee Surgery, Sport Traumatol Arthrosc. 2013;21(12):2659–60.

3. Kumar D, Manal KT, Rudolph KS. Knee joint loading during gait in healthy controls and individuals with knee osteoarthritis. Osteoarthr Cartil [Internet]. 2013;21(2):298–305. Available from: http://dx.doi.org/10.1016/j.joca.2012.11.008

4. Brouwer GM, Van Tol AW, Bergink AP, Belo JN, Bernsen RMD, Reijman M, et al. Association between valgus and varus alignment and the development and progression of radiographic osteoarthritis of the knee. Arthritis Rheum. 2007;56(4):1204–11.

5. Sharma L, Song J, Dunlop D, Felson D, Lewis CE, Segal N, et al. Varus and valgus alignment and incident and progressive knee osteoarthritis. Ann Rheum Dis [Internet]. 2010 Nov;69(11):1940–5. Available from: https://ard.bmj.com/lookup/doi/10.1136/ard.2010.129742

6. Sharma L, Chmiel JS, Almagor O, Felson D, Guermazi A, Roemer F, et al. The role of varus and valgus alignment in the initial development of knee cartilage damage by MRI: the MOST study. Ann Rheum Dis [Internet]. 2013 Feb;72(2):235–40. Available from: https://ard.bmj.com/lookup/doi/10.1136/annrheumdis-2011-201070

7. KELLGREN JH, LAWRENCE JS. Radiological assessment of osteo-arthrosis. Ann Rheum Dis [Internet]. 1957 Dec;16(4):494–502. Available from: http://www.ncbi.nlm.nih.gov/pubmed/13498604

8. Kohn MD, Sassoon AA, Fernando ND. Classifications in Brief: Kellgren-Lawrence Classification of Osteoarthritis. Clin Orthop Relat Res. 2016;474(8):1886–93.

9. Felson DT, Hodgson R. Identifying and treating preclinical and early osteoarthritis. Rheum Dis Clin North Am. 2014;40(4):699–710.

10. Dessery Y, Belzile ÉL, Turmel S, Corbeil P. Comparison of three knee braces in the treatment of medial knee osteoarthritis. Knee [Internet]. 2014;21(6):1107–14. Available from: http://dx.doi.org/10.1016/j.knee.2014.07.024

11. Haladik JA, Vasileff WK, Peltz CD, Lock TR, Bey MJ. Bracing improves clinical outcomes but does not affect the medial knee joint space in osteoarthritic patients during gait. Knee Surgery, Sport Traumatol Arthrosc. 2014;22(11):2715–20.

12. Chen P, Gao L, Shi X, Allen K, Yang L. Fully automatic knee osteoarthritis severity grading using deep neural networks with a novel ordinal loss. Comput Med Imaging Graph [Internet]. 2019;75:84–92. Available from: https://doi.org/10.1016/j.compmedimag.2019.06.002

13. Dettoni F, Bonasia DE, Castoldi F, Bruzzone M, Blonna D, Rossi R. High tibial osteotomy versus unicompartmental knee arthroplasty for medial compartment arthrosis of the knee: a review of the literature. Iowa Orthop J [Internet]. 2010;30:131–40. Available from: http://www.ncbi.nlm.nih.gov/pubmed/21045985

14. Cao ZW, Mai XJ, wang J, Feng EH, Huang YM. Uni-compartmental knee arthroplasty versus

high tibial osteotomy for knee osteoarthritis: a systematic review and meta-analysis. J Arthroplasty [Internet]. 2018;33(3):952–9. Available from: https://doi.org/10.1016/j.arth.2017.10.025

15. Lobenhoffer P, Agneskirchner JD. Umstellungsosteotomie vs. unikondyläre Prothese bei Gonarthrose. Orthopade. 2014;43(10):923–9.

16. Dettoni F, Maistrelli GL, Stojimirovic D, Bonasia DE, Bruzzone M, Castoldi F. Treatment of medial unicompartmental arthritis of the knee: high tibial osteotomy versus unicompartmental arthroplasty. 2–4- year follow-up prospective study. In: Journal of Orthopaedics and Traumatology. 2008. p. 1–94.

17. W-Dahl A, Robertsson O, Lidgren L. Surgery for knee osteoarthritis in younger patients: A Swedish register study. Acta Orthop. 2010;81(2):161–4.

18. Thambiah MD, Tan MKL, Hui JHP. Role of High Tibial Osteotomy in Cartilage Regeneration - Is Correction of Malalignment Mandatory for Success? Indian J Orthop [Internet]. 2018;51(5):588–99. Available from: http://www.ncbi.nlm.nih.gov/pubmed/28966382

19. Ferruzzi A, Buda R, Cavallo M, Timoncini A, Natali S, Giannini S. Cartilage repair procedures associated with high tibial osteotomy in varus knees: Clinical results at 11years' follow-up. Knee [Internet]. 2014;21(2):445–50. Available from: http://dx.doi.org/10.1016/j.knee.2013.11.013

20. Faber S, Angele P, Zellner J, Bode G, Hochrein A, Niemeyer P. Comparison of Clinical Outcome following Cartilage Repair for Patients with Underlying Varus Deformity with or without Additional High Tibial Osteotomy: A Propensity Score–Matched Study Based on the German Cartilage Registry (KnorpelRegister DGOU). Cartilage. 2020;

21. Caron JJ, Custers RJH, Emans PJ. Chirurgische behandeling van (osteo) chondrale defecten in de knie. Ned Orthop Ver. 2019;https://ww:1–41.

22. Bedi A, Haidukewych GJ. Management of the posttraumatic arthritic knee. J Am Acad Orthop Surg. 2009;17(2):88–101.

23. Smith JO, Wilson AJ, Thomas NP. Osteotomy around the knee: Evolution, principles and results. Knee Surgery, Sport Traumatol Arthrosc. 2013;21(1):3–22.

24. Agarwala S, Sobti A, Naik S, Chaudhari S. Comparison of closing-wedge and opening-wedge high tibial osteotomies for medial compartment osteoarthritis of knee in Asian population: Mid-term follow-up. J Clin Orthop Trauma [Internet]. 2016;7(4):272–5. Available from: http://dx.doi.org/10.1016/j.jcot.2016.06.012

25. Hankemeier S, Mommsen P, Krettek C, Jagodzinski M, Brand J, Meyer C, et al. Accuracy of high tibial osteotomy: Comparison between open- and closed-wedge technique. Knee Surgery, Sport Traumatol Arthrosc. 2010;18(10):1328–33.

26. Brinkman JM, Lobenhoffer P, Agneskirchner JD, Staubli AE, Wymenga AB, Van Heerwaarden RJ. Osteotomies around the knee: Patient selection, stability of fixation and bone healing in high tibial osteotomies. J Bone Jt Surg - Ser B. 2008;90(12):1548–57.

27. Nguyen HC, Gielis WP, van Egmond N, Weinans H, Slump CH, Sakkers RJB, et al. The need for a standardized whole leg radiograph guideline: The effects of knee flexion, leg rotation, and X-ray beam height. J Cartil Jt Preserv [Internet]. 2021;(August):100022. Available from: https://doi.org/10.1016/j.jcjp.2021.100022

28. Chang J, Scallon G, Beckert M, Zavala J, Bollier M, Wolf B, et al. Comparing the accuracy of

high tibial osteotomies between computer navigation and conventional methods. Comput Assist Surg [Internet]. 2017 Jan 4;22(1):1–8. Available from: https://www.tandfonline.com/doi/full/10.1080/24699322.2016.1271909

29. Paley D. Principles of Deformity Correction. Springer-Verlag Berlin and Heidelberg GmbH & Co. KG; 2002. 816 p.

30. Lee DC, Byun SJ. High Tibial Osteotomy. Knee Surg Relat Res [Internet]. 2012 Jun 30;24(2):61–9. Available from: http://www.jksrr.org/journal/view.html?doi=10.5792/ksrr.2012.24.2.61

31. Fujisawa Y, Masuhara K, Shiomi S. The effect of high tibial osteotomy on osteoarthritis of the knee. An arthroscopic study of 54 knee joints. Orthop Clin North Am [Internet]. 1979 Jul;10(3):585–608. Available from: http://www.ncbi.nlm.nih.gov/pubmed/460834

32. Gao L, Madry H, Chugaev D V., Denti M, Frolov A, Burtsev M, et al. Advances in modern osteotomies around the knee: Report on the Association of Sports Traumatology, Arthroscopy, Orthopaedic surgery, Rehabilitation (ASTAOR) Moscow International Osteotomy Congress 2017. J Exp Orthop. 2019;6(1).

33. Jud L, Roth T, Roth T, Fürnstahl P, Vlachopoulos L, Sutter R, et al. The impact of limb loading and the measurement modality (2D versus 3D) on the measurement of the limb loading dependent lower extremity parameters. BMC Musculoskelet Disord. 2020;21(1):1–9.

34. León-Muñoz VJ, López-López M, Martínez-Martínez F, Santonja-Medina F. Comparison of weight-bearing full-length radiographs and computed-tomography-scan-based three-dimensional models in the assessment of knee joint coronal alignment. Knee. 2020;27(2):543–51.

35. Conti MS, Ellis SJ. Weight-bearing CT Scans in Foot and Ankle Surgery. J Am Acad Orthop Surg. 2020;28(14):e595–603.

36. Fucentese SF, Meier P, Jud L, Köchli GL, Aichmair A, Vlachopoulos L, et al. Accuracy of 3D-planned patient specific instrumentation in high tibial open wedge valgisation osteotomy. J Exp Orthop. 2020;7(1).

37. Mao Y, Xiong Y, Li Q, Chen G, Fu W, Tang X, et al. 3D-Printed Patient-Specific Instrumentation Technique Vs . Conventional Technique in Medial Open Wedge High Tibial Osteotomy : A Prospective Comparative Study. 2020;2020.

38. Markelj P, Tomaževič D, Likar B, Pernuš F. A review of 3D/2D registration methods for image-guided interventions. Med Image Anal. 2012;16(3):642–61.

39. Rchoetzlein. Elements of polygonal mesh modeling [Internet]. 2009 [cited 2021 Oct 18]. Available from: https://en.wikipedia.org/wiki/Polygon_mesh

40. Saffarini M, Nover L, Tandogan R, Becker R, Moser LB, Hirschmann MT, et al. The original Akagi line is the most reliable: a systematic review of landmarks for rotational alignment of the tibial component in TKA. Knee Surgery, Sport Traumatol Arthrosc [Internet]. 2019;27(4):1018–27. Available from: http://dx.doi.org/10.1007/s00167-018-5131-z

41. Koo TK, Li MY. A Guideline of Selecting and Reporting Intraclass Correlation Coefficients for Reliability Research. J Chiropr Med [Internet]. 2016;15(2):155–63. Available from: http://dx.doi.org/10.1016/j.jcm.2016.02.012

42. Rusinkiewicz S, Levoy M. Efficient variants of the ICP algorithm. Proc Int Conf 3-D Digit Imaging Model 3DIM. 2001;145–52.

43. Wang K. Computational Intelligence in Agile Manufacturing Engineering [Internet]. Agile

Manufacturing: The 21st Century Competitive Strategy. Elsevier Science Ltd.; 2001. 297–315 p. Available from: http://dx.doi.org/10.1016/B978-0-08-043567-1.50016-4

44. Gutmann HM. A Radial Basis Function Method for Global Optimization. J Glob Optim. 2001;19(3):201–27.

45. Wang Y, Shoemaker CA. A General Stochastic Algorithmic Framework for Minimizing Expensive Black Box Objective Functions Based on Surrogate Models and Sensitivity Analysis. 2014; Available from: http://arxiv.org/abs/1410.6271

46. Ascione F, Bianco N, De Stasio C, Mauro GM, Vanoli GP. Energy Management in Hospitals [Internet]. Vols. 5–5, Comprehensive Energy Systems. Elsevier Ltd.; 2018. 827–854 p. Available from: http://dx.doi.org/10.1016/B978-0-12-809597-3.00541-1

47. Lindner C, Thiagarajah S, Wilkinson JM, Wallis GA, Cootes TF. Fully automatic segmentation of the proximal femur using random forest regression voting. IEEE Trans Med Imaging. 2013;32(8):1462–72.

48. Lindner C, Thiagarajah S, Wilkinson JM, Wallis GA, Cootes TF. Accurate Bone Segmentation in 2D Radiographs Using Fully Automatic Shape Model Matching Based On Regression-Voting. In 2013. p. 181–9. Available from: http://link.springer.com/10.1007/978-3-642-40763-5_23

49. van Eijnatten M, van Dijk R, Dobbe J, Streekstra G, Koivisto J, Wolff J. CT image segmentation methods for bone used in medical additive manufacturing. Med Eng Phys [Internet]. 2018;51(November):6–16. Available from: https://doi.org/10.1016/j.medengphy.2017.10.008

50. Schröter S, Ihle C, Mueller J, Lobenhoffer P, Stöckle U, van Heerwaarden R. Digital planning of high tibial osteotomy. Interrater reliability by using two different software. Knee Surgery, Sport Traumatol Arthrosc. 2013;21(1):189–96.

51. Hamadeh A, Lavallee S, Cinquin P. Automated 3-dimensional computed tomographic and fluoroscopic image registration. Comput Aided Surg. 1998;3(1):11–9.

52. Zuffi S, Leardini A, Catani F, Fantozzi S, Cappello A. A model-based method for the reconstruction of total knee replacement kinematics. IEEE Trans Med Imaging. 1999;18(10):981–91.

53. Yamazaki T, Watanabe T, Nakajima Y, Sugamoto K, Tomita T, Yoshikawa H, et al. Improvement of depth position in 2-D/3-D registration of knee implants using single-plane fluoroscopy. IEEE Trans Med Imaging [Internet]. 2004 May;23(5):602–12. Available from: http://www.ncbi.nlm.nih.gov/pubmed/15147013

54. Huda W, Abrahams RB. X-Ray-Based Medical Imaging and Resolution. Am J Roentgenol [Internet]. 2015 Apr;204(4):W393–7. Available from: http://www.ajronline.org/doi/10.2214/AJR.14.13126

55. Roth T, Carrillo F, Wieczorek M, Ceschi G, Esfandiari H, Sutter R, et al. Three-dimensional preoperative planning in the weight-bearing state: validation and clinical evaluation. Insights Imaging [Internet]. 2021;12(1). Available from: https://doi.org/10.1186/s13244-021-00994-8

56. Bergström P, Edlund O. Robust registration of point sets using iteratively reweighted least squares. Comput Optim Appl. 2014;58(3):543–61.

57. Bergström P, Edlund O. Robust registration of surfaces using a refined iterative closest point algorithm with a trust region approach. Numer Algorithms. 2017;74(3):755–79.

APPENDIX

Data creation and validation

Data creation

A dataset with 60 CT scans of the lower limbs was available for this study. The decision was made to include 30 patients for this research. The first 30 patients in chronological order were included from the dataset.

From the CT scans anatomical models of the femur and tibia were segmented using Mimics v23.0 (Materialise NV., Leuven, Belgium). The position and orientation of the coordinates of the 3D models was changed from the coordinate system used in the CT scan to the 3D cartesian coordinate system. This ensures compatibility with the 2D DRR and MatLab. Figure A1 shows the difference between the two coordinate systems. Information from the DICOM tags, located within the CT scan files, was used to align the origin points of the CT scan, 3D models, and the DRR.

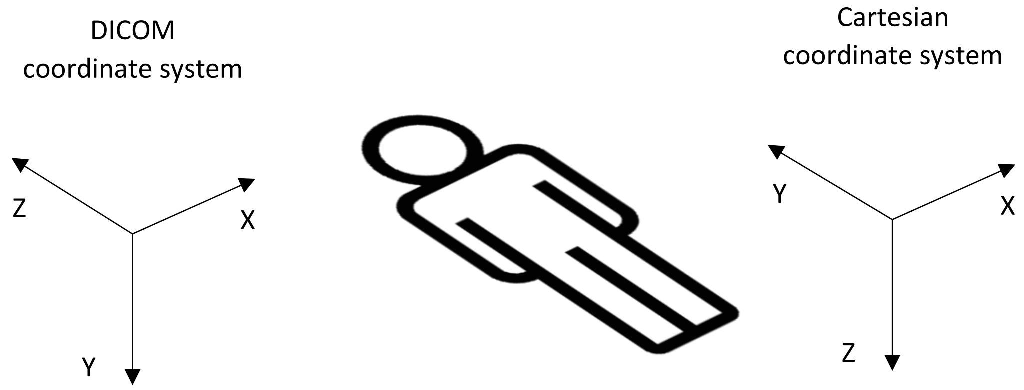

FIGURE A1: THE COORDINATE SYSTEMS USE BY THE DICOM IMAGES FROM THE CT SCAN AND THE CARTESIAN COORDINATE SYSTEM. THE X-AXIS AND THE Y-AXIS DENOTE DIFFERENT LOCATIONS BETWEEN EACH SYSTEM.

The CT scans were used to create the digital reconstructed radiograph (DRR). This was done using MeVisLab. One of the challenges was to remove the CT bed from the DRR. This was done by segmenting the patient in the CT scan using a region growing process and morphological operators to separate and segment the patient from the bed. The complete set of steps taken to achieve the segmentation and to create the DRR were:

1. The CT scan is imported.
2. The CT scan is eroded with a 3x3x3 pixel kernel to cut connections between the patient and the CT bed.
3. A region growing process is performed to segment the patient from the CT scan. Initial seed point is placed in one of the legs.
4. The 3D mask is dilated with a 3x3x3 pixel kernel to recover correct size of the mask.
5. The mask is used to keep the patient in the CT scan and remove everything that is not the patient.
6. The y-axis is flipped to ensure the DRR is made in the anteroposterior position.
7. The DRR is made using a built-in lookup table (LUT) for optimal and realistic contrast in the DRR.
8. The DRR is saved to a folder.

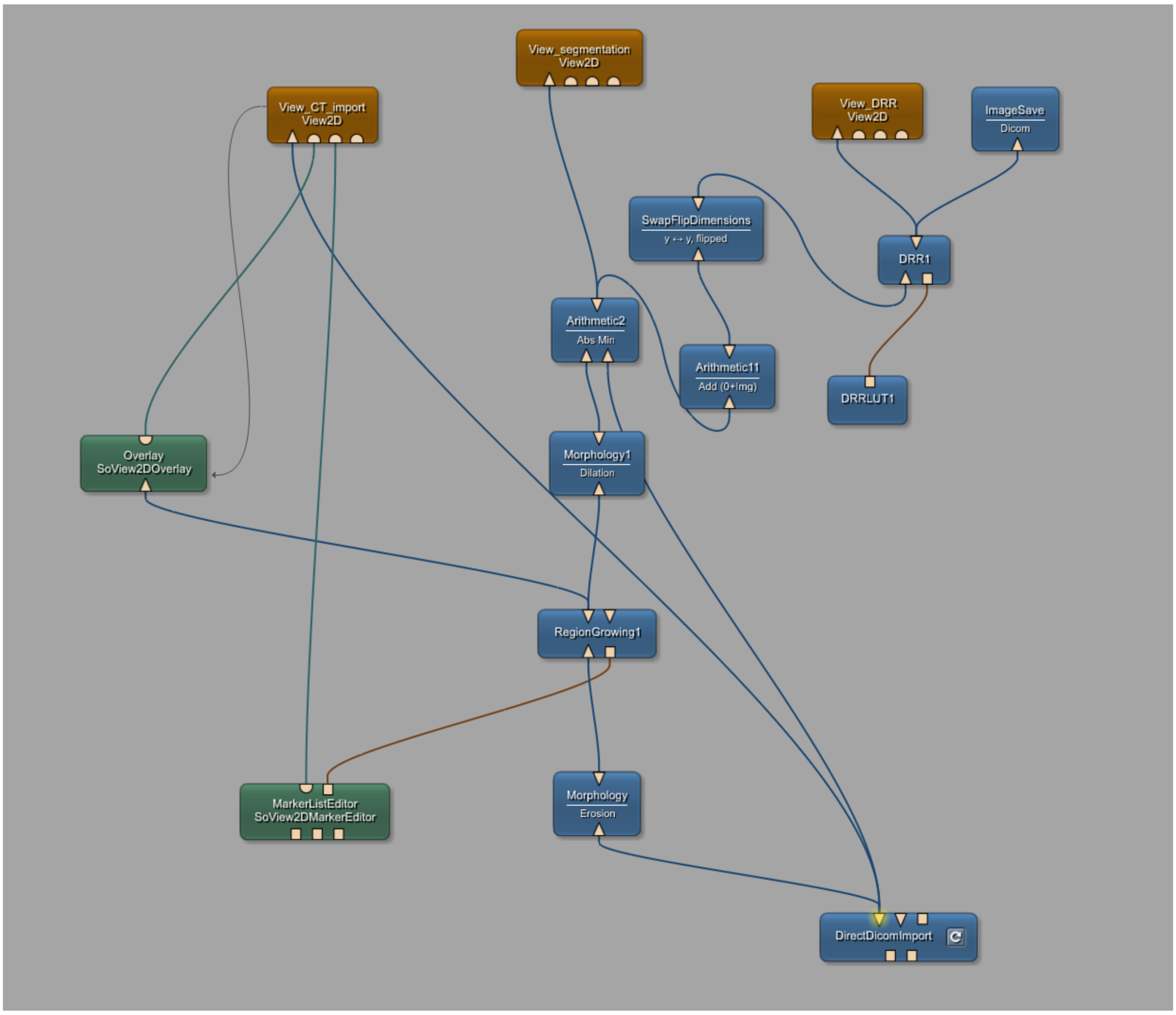

FIGURE A2: THE STEPS TAKEN TO ACQUIRE DRRS FROM THE CT SCANS

Data validation

The DRRs were validated using a CT scan without data, except for a solid bar with intensity of 5000 Hounsfield units. This CT scan was used to create a DRR. The location of the bar in the CT scan was known and the parameters used for the DRR known, the location of the edges of the bar in the DRR could be calculated using formula 1.

The calculated position of the edges of the bar in the DRR were compared with the measured location of the edges of the bar. These were found to be identical.

With this test we could conclude that the DRRs created were valid to the results as we previously had calculated. The DRRs could therefore be used as a substitute for real WLRs.

Semi-automatic registration algorithm

The semi-automatic registration algorithm was constructed in MatLab. It was built in two steps: a coarse registration step and a fine iterative registration step.

After loading in the DRR and the 3D models, the first task was to mark a few anatomical landmarks and to mark the contour of the bones in the WLR. As described in the chapter Method, the contour was once derived from the reference 3D models, and once marked by the user. Figure A3 shows the markers for one patient from both methods.

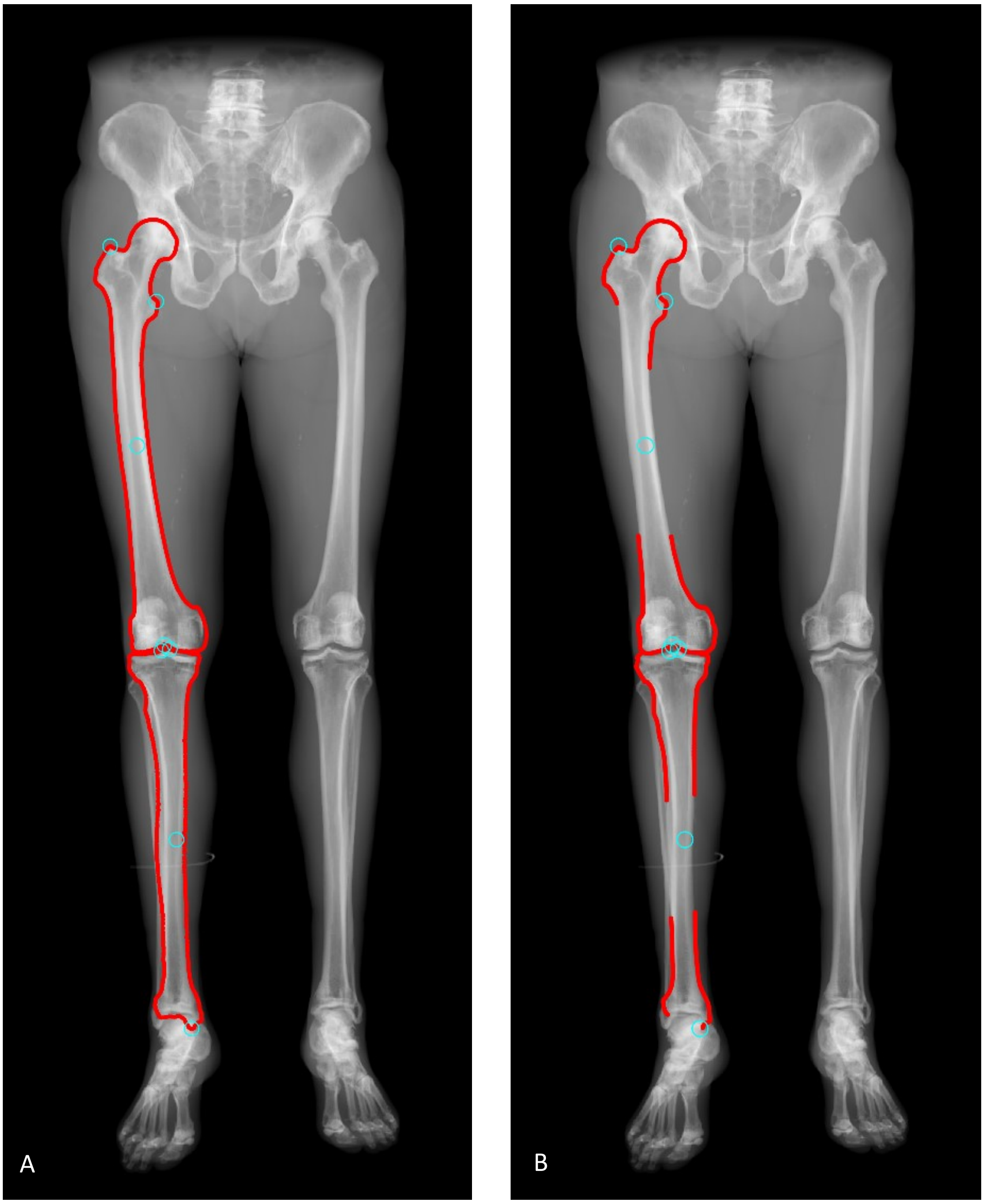

FIGURE A3: THE CONTOUR OF FEMUR AND TIBIA IN RED FROM A) THE REFERENCE MODEL, AND B) THE USER MARKING. THE ANATOMICAL LANDMARKS ARE THE CYAN CIRCLES. THESE WERE THE SAME FOR BOTH METHODS.

The anatomical landmarks were also selected on the 3D model of the femur and tibia. Additional markers were calculated at halfway between the two most vertical markers for both the femur and tibia. With these markers, and the vectors between these markers, the coarse registration could be performed.

First the two horizontal vectors were aligned between 3D model and the WLR.

```
%% Rotate and align vectors
Define direction of vector between landmarks on 2D image

Define direction of vector between landmarks on 3D model

Calculate rotation matrix to align the two vectors

Apply rotation matrix to the 3D model and markers
```

After this step, the two vertical vectors (and WLR and 3D model) were aligned. These vectors are between the trochanter major and the femoral notch for the femur, and between the lateral eminence and the distal point of the tibia for the tibia. The same code as for the first alignment can be adjusted and used.

The difference in length between the vertical vectors can be used to calculate the approximate sagittal position of the femur.

```
%% Determine approximate Z-position
Calculate length of the bone between vertical vectors on 2D WLR
Calculate length of the bone between vertical vectors on 3D model
Calculate ratio between length in 2D and 3D

Calculate the z-positions of the femur using formula 1 and the ratio of
lengths

Translate tibia to new z-position
```

After the models have been aligned with the WLR, and the approximate sagittal position has been calculated and applied, the models can be roughly registered based on one of the anatomical markers for each model: the trochanter major and the lateral eminence.

```
%% Registration Troch-Troch and Emi-Emi
Calculate the magnification of the projection at the current Z-position

Translate 3D models to the centre of image

Calculate translation of 3D model, using projection magnification and
difference in position of 3D model and 2D WLR

Translate 3D model with the calculated translation
```

The results from the coarse registration are then used as input for the optimization algorithm. Figure A4 show the results from the coarse registration in the frontal plane and the sagittal plane, with the projection applied to the 3D model. While the registration looks accurate in the frontal plane, the sagittal plane shows the misalignment between femur and tibia.

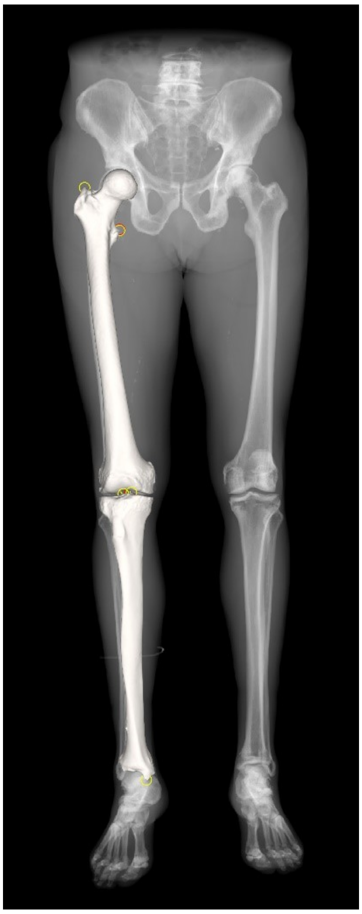

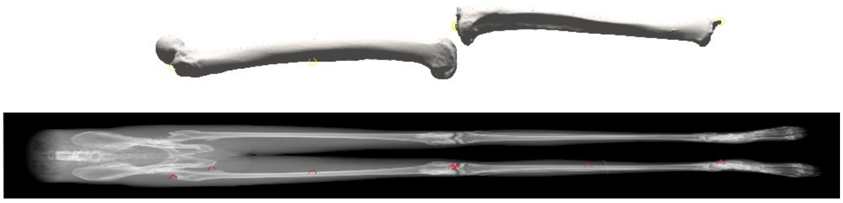

FIGURE A4: THE MODELS AFTER THE COARSE REGISTRATION STEPS SEEM TO ALIGN WITH THE WLR IN THE FRONTAL PLANE, BUT THE SAGITTAL PLANE REVEALS THAT THE MODELS ARE STILL MISALIGNED.

The final step in the semi-automatic registration algorithm is the optimization algorithm. The optimization algorithm will calculate the optimum for the variables where the optimization metric will be minimum.

```
%% Optimization algorithm
Define variables, bounds, constraints and optimization options

Define the optimization function
      Translate 3D model in Z-direction
      Rotate 3D model around internal X-axis
      Rotate 3D model around internal Y-axis

      Define 2D contour of 3D model
      Apply ICP algorithm to register contour of 3D model to contour in
      WLR

      Calculate the distance between centre of distal femur and proximal
      tibia
      Calculate optimization metric
            Maximum value of distances between nearest neighbours of 3D
            contour and 2D contour

Define the constraint function
      Distance between centre of distal femur and centre of proximal
      tibia cannot be more than 10mm in Z-direction

      Femoral notch must lie below later eminence in frontal plane

      Distance between femoral notch and lateral eminence cannot be more
      than 15mm in Y-direction
```

Comparison of manual & semi-automatic registration

The tables and graphs below further compare the results between the average results of the manual registration and the results from the three different optimization algorithms, used in the semi-automatic registration. Table A1 further show how the results, as already described in the chapter Results, are worse for the semi-automatic registration, compared to the manual registration.

TABLE A1: THE DISTANCE ERRORS IN THE XYZ DIMENSION BETWEEN THE DIFFERENT REGISTRATION METHODS. DISTANCES IN MILLIMETER.

	Manual		**Genetic Algorithm**		**Multi obj. GA**		**Surrogate**	
	Femur	**Tibia**	**Femur**	**Tibia**	**Femur**	**Tibia**	**Femur**	**Tibia**
1	4.05	4.24	14.78	52.32	13.44	8.64	19.64	19.60
2	3.24	5.91	11.90	12.35	4.35	4.19	32.21	41.93
3	5.84	7.37	13.22	10.75	7.24	8.99	14.51	11.99
4	6.80	5.17	27.08	6.13	27.50	12.62	39.36	13.71
5	3.16	6.53	79.16	94.97	30.99	5.11	35.24	11.74
6	5.96	5.61	7.42	8.44	13.55	4.49	56.62	66.91
7	7.89	4.69	32.77	44.21	20.50	19.40	44.35	31.84
8	4.38	3.90	45.57	33.52	16.50	7.11	20.92	22.52
9	9.44	6.31	30.73	7.20	15.83	17.51	80.01	70.39
10	4.27	4.09	27.48	42.09	12.04	6.57	17.93	24.68
Average	**5.50**	**5.38**	**29.01**	**31.20**	**16.19**	**9.46**	**36.08**	**31.53**

Figure A5 visualizes how the manual registration consistently achieves higher SDCs. As discussed earlier, while a high SDC does not denote an accurate registration, it is indicative of the registration accuracy

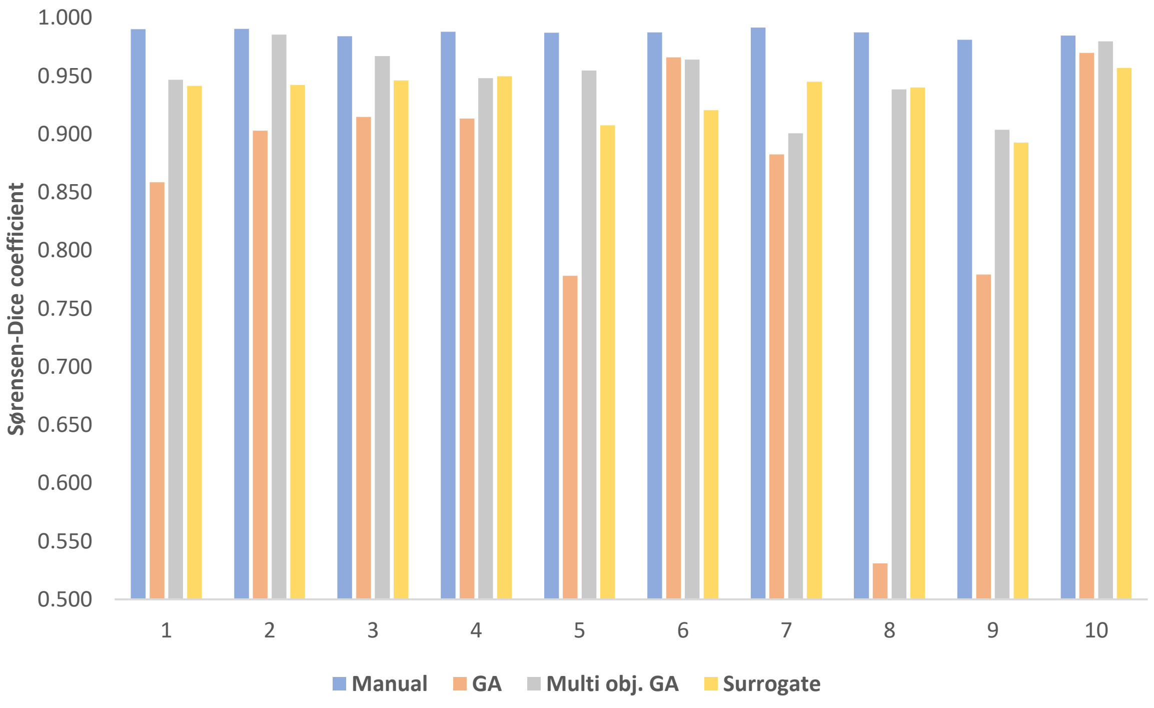

FIGURE A5: THE SØRENSEN-DICE COEFFICIENT OF THE DIFFERENT REGISTRATION METHODS AND ALGORITHMS.

Figure A6 visualizes the distribution in angular difference between reference and registered models. The figure shows how the optimization algorithms have wider ranges of angular differences, compared to the manual registration.

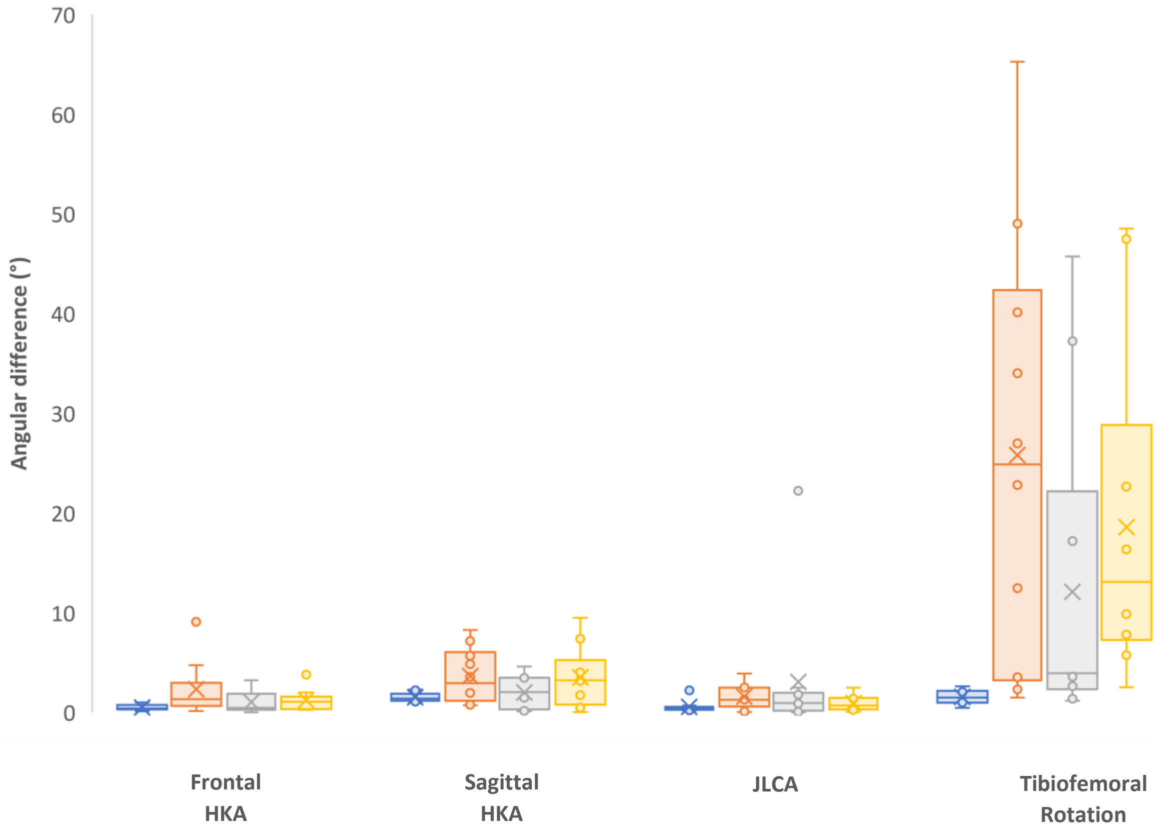

FIGURE 19: THE DISTRIBUTION OF THE DIFFERENCES IN MEASURED ANGLES BETWEEN REFERENCE AND REGISTERED MODELS FOR ALL RATERS. THE BLUE BOXPLOTS = MANUAL REGISTRATION, ORANGE = GENETIC ALGORITHM, GREY = MULTI OBJ. GA, YELLOW = SURROGATE ALGORITHM. HKA = HIP-KNEE-ANKLE ANGLE, JLCA = JOINT LINE CONVERSION ANGLE.